Regulatory Role of Astrocyte-Expressed Fatty Acid Binding Protein 7 (FABP7) on Morphology and Synaptic Plasticity of Cortical Neurons

（アストロサイトに発現する脂肪酸結合タンパク質（FABP7）は、大脳皮質神経細胞の形態と神経可塑性調節に関与する）

氏名　Majid Ebrahimi

所属　山口大学大学院医学系研究科

システム統御医学系専攻　器官解剖学分野

平成２７年　１月

Regulatory Role of Astrocyte-Expressed Fatty Acid Binding Protein 7 (FABP7) on Morphology and Synaptic Plasticity of Cortical Neurons

by

Majid Ebrahimi

A dissertation

in

Cellular and Molecular Neuroscience

Presented to the faculties of Yamaguchi University Graduate School of Medicine

in

Partial fulfillment of the requirements for the degree of doctor of philosophy (PhD)

Supervisor of Dissertation

Yuji Owada, M.D., Ph.D.

Dissertation committee

Michiyasu Suzuki, M.D., Ph.D.

Dai Mitsushima, D.V.M., Ph.D.

2015

ABSTRACT

Fatty acid binding protein 7 (FABP7) expressed by astrocytes in developing and mature brains is involved in uptake and transportation of fatty acids, signal transduction, and gene transcription. *Fabp7* knockout (*Fabp7* KO) mice show behavioral phenotypes reminiscent of human neuropsychiatric disorders such as schizophrenia. However, direct evidence showing how FABP7 deficiency in astrocytes leads to behavioral impairments is lacking.

Here, we examined neuronal dendritic morphology and synaptic plasticity in medial prefrontal cortex (mPFC) of *Fabp7* KO mice and in primary cortical neuronal cultures. Golgi staining of cortical pyramidal neurons in *Fabp7* KO mice revealed aberrant dendritic morphology and decreased spine density compared with those in wild-type (WT) mice. Aberrant dendritic morphology was also observed in primary cortical neurons co-cultured with FABP7-deficient astrocytes and neurons cultured in *Fabp7* KO astrocyte-conditioned medium. Excitatory synapse number was decreased in the mPFC of *Fabp7* KO mice and in neurons co-cultured with *Fabp7* KO astrocytes. Accordingly, whole-cell voltage-clamp recording in brain slices from pyramidal cells in the mPFC showed that both amplitude and frequency of action potential-independent miniature excitatory postsynaptic currents (mEPSCs) were decreased in *Fabp7* KO mice. Moreover, transplantation of WT astrocytes into the mPFC of *Fabp7* KO mice partially attenuated behavioral impairments. To further explore the mechanistic roles of FABP7 on astrocyte function, the proteome of astrocytes cultured from *Fabp7* KO mice was compared with WT counterparts by two-dimensional gel electrophoresis (2-DE), and selected spots were

analyzed using liquid chromatography tandem mass spectrometry (LC-MS/MS) analysis. As a result, vimentin and PEA-15 were identified to be downregulated in *Fabp7* KO astrocytes.

Collectively, these results suggest that astrocytic FABP7 is important for dendritic arbor growth, neuronal excitatory synapse formation, and synaptic transmission in cortical neurons, and FABP7 has regulatory role on astrocyte proteome. These findings provide new insights linking FABP7, lipid homeostasis, and CNS disorders and may lead to novel therapeutic interventions.

Keywords: 2-DE, astrocyte, FABP7, glia, glioma, hyperactivity, mEPSCs, mPFC, LC-MS/MS, PEA-15, vimentin

TABLE OF CONTENTS

TITLE PAGE..... i
ABSTRACT..... ii
TABLE OF CONTENTS..... vi
LIST OF TABLES..... v
LIST OF ILLUSTRATIONS..... v

1. INTRODUCTION..... 1
1.1. Glial cells constitute most of the cells in the brain..... 1
1.2. Astrocytes multi-functional glial cells..... 1
1.3. Astrocytes dysfunction and disease..... 3
1.4. Fatty acid binding proteins (FABPs), a family of intracellular chaperons for lipophilic molecules..... 4
1.5. FABP7, a glia-expressed FABP..... 6
1.6. Neuronal morphology and dendritic structures..... 7
1.7. Altered neuronal morphology in neurological disorders..... 8
1.8. Aim of present study..... 9
2. MATERIALS AND METHODS..... 11
2.1. Animals..... 11
2.2. Neuron-enriched primary mixed cortical cultures..... 11
2.3. Primary cortical neuron-astrocyte co-cultures..... 13
2.4. Preparation of astrocyte-conditioned medium (ACM) and cortical neuronal cultures with ACM..... 15
2.5. Immunohistochemistry..... 16
2.6. Golgi staining and in vivo assessment of neuronal morphology..... 18
2.7. Immunocytochemistry and assessment of neuronal morphology..... 20
2.8. Quantification of synapse number..... 21
2.9. Electrophysiology..... 24
2.10. Behavioral tests and cell transplantation..... 25
2.11. Preparation of protein samples for Proteomic differential display analysis..... 26
2.12. 2-DE analysis..... 27
2.13. Image analysis and spot picking and in gel digestion..... 28
2.14. LC-MS/MS analysis..... 29
2.15. Western blotting..... 29
2.16. Statistics..... 29
3. RESULTS..... 31
3.1. Dendritic complexity and spine density is altered in the prefrontal cortex of FABP7-deficient mice..... 31

3.2. Neuronal morphology is altered in FABP7-deficient neuron-enriched mixed cortical cultures…….. 36
3.3. Neuronal morphology is altered in FABP7-deficient neuron-astrocyte co-cultures…. 38
3.4. Neuronal morphology is altered in cortical neurons cultured with ACM derived from FABP7-deficient astrocytes……... 40
3.5. FABP7 deficiency in astrocytes impairs synapse formation……. 42
3.6. Excitatory synaptic transmission is decreased in the mPFC of FABP7-deficient mice 44
3.7. Transplantation of WT astrocytes rescues altered behavioral phenotypes in FABP7-deficient mice……. 46
3.8. Detection of spots with differential expression between WT and Fabp7 KO astrocytes on 2-DE gels..... 48
3.9. Identification of proteins..... 49
3.10. Decreased expression of vimentin and PEA-15 in Fabp7 KO astrocytes..... 50
4. DISCUSSION……... 52
REFERENCES……. 59

LIST OF TABLES

Table 2.1 Information of primary antibodies utilized in this study…… 18
Table 3.1 Table 3.1. Identification of proteins that are differentially expressed between *Fabp7* KO and WT astrocytes by LC-MS/MS analysis..... 49

LIST OF ILLUSTRATIONS

Fig. 1.1 Glial cells in the CNS and their interactions with surrounding cells…….. 2
Fig. 1.2 Cellular functions of FABPs…… 4
Fig. 1.3 Phylogenetic tree of fatty acid binding protein members of human…… 5
Fig. 1.4 Several overlapping processes towards development of dendritic arbor……. 8
Fig. 2.1 Neuron-enriched primary mixed cortical culture……. 12
Fig. 2.2 Primary cortical neuron-astrocyte co-culture…….. 14
Fig. 2.3 Scheme shows preparation of cortical neuronal cultures with ACM…….. 16
Fig. 2.4 Location of mPFC in the mouse brain and representative image of Golgi staining of mPFC in the mouse brain…… 19
Fig. 2.5 Neuronal morphological parameters evaluated using NeuronMetrics…… 21
Fig. 2.6 Outline of experiment for transplantation of astrocytes in to the mPFC of *Fabp7* 26

KO mice……...
Fig. 3.1 Identification of FABP7-expressing cells in the mPFC of normal mouse brain…. 31
Fig. 3.2 The population density of neural cells in the mPFC of Fabp7 KO mice……. 32
Fig. 3.3 Alteration of neuronal dendritic morphology in the mPFC of Fabp7 KO mice….. 34
Fig. 3.4 Alteration of density and maturity of dendritic spines in the mPFC of FABP7-deficient mice……... 35
Fig. 3.5 Viability of neurons in culture is not influenced by FABP7 deficiency……. 36
Fig. 3.6 Alteration of neuronal morphology in FABP7-deficient neuron-enriched primary mixed cortical cultures…… 37
Fig. 3.7 Alteration of neuronal morphology in FABP7-deficient neuron-astrocyte co-culture…….. 39
Fig. 3.8 No significant difference is detected in the population density of astrocytes between WT and FABP7-deficient co-cultures……... 40
Fig. 3.9 No significant difference is detected in population densities from cortical neurons cultured with ACM derived from WT or FABP7-deficient astrocytes….. 41
Fig. 3.10 Alteration of neuronal morphology in cortical neurons cultured with ACM prepared from FABP7-deficient astrocytes……. 42
Fig. 3.11 Alteration of excitatory synapse formation in the mPFC of *Fabp7* KO mice……. 43
Fig. 3.12 Alteration of excitatory synapse formation in the cortical neurons co-cultured with FABP7-deficient astrocytes……. 44
Fig. 3.13 Excitatory synaptic transmission is decreased in pyramidal neurons in the mPFC of FABP7-deficient mice……. 45
Fig. 3.14 Astrocyte transplantation partially rescues behavioral phenotype in *Fabp7* KO mice…… 47
Fig. 3.15 Representative images of 2-DE gels of WT and *Fabp7* KO astrocytes stained with fluorescent dye (Flamingo Gel Stain)..... 48
Fig. 3.16 Protein levels of FABP7, GFAP, PEA-15 and vimentin in WT and *Fabp7* KO astrocytes were evaluated by Western blotting..... 50

1. INTRODUCTION

1.1. Glial cells constitute most of the cells in the brain

The central nervous system (CNS) is made up of two main cell types namely neurons and glia. Of interest, glial cells constitute up to 90% of cells population in the human brain. They adopted their name from the Greek word for glue, but now it is apparent that they do not just hold nerve cells together and hence should not just be regarded as supportive cells to neurons. Recent compelling evidence indicates that glial cells play active and crucial roles in the development and function of the brain (1, 2).

There are three types of glial cells exist in the CNS: astrocytes, oligodendrocytes and microglia. Astrocytes are the most abundant glial cells with star-shaped cell bodies and extensive endfeet on their processes. They involve in the brain homeostasis, interact extensively with neurons and provide them with important structural, metabolic support and substrates for neurotransmission. Oligodendrocytes have several processes which wrap themselves around neuronal axons to form myelin sheaths, which enwrap axons, thereby speeding up the conduction of electrical impulses. Microglia, the smallest of the glial cells, are resident immune cells of the CNS, which act as phagocytes survey the brain for damage and infection, engulfing dead cells and debris [**Fig. 1.1]** (1, 3).

1.2. Astrocytes multi-functional glial cells

Astrocytes play important roles in normal brain organization through guidance of neuronal development, homeostatic synaptic scaling and modulation of neurophysiological mechanisms implicated in the regulation of complex behavioral processes (4-6). Currently, there is no doubt

that astrocytes are dynamically involved in antioxidant defense, inflammatory response, metabolic and ionic homeostasis, synaptic transmission, trophic support of neurons, and the establishment and maintenance of the blood-brain barrier (7).

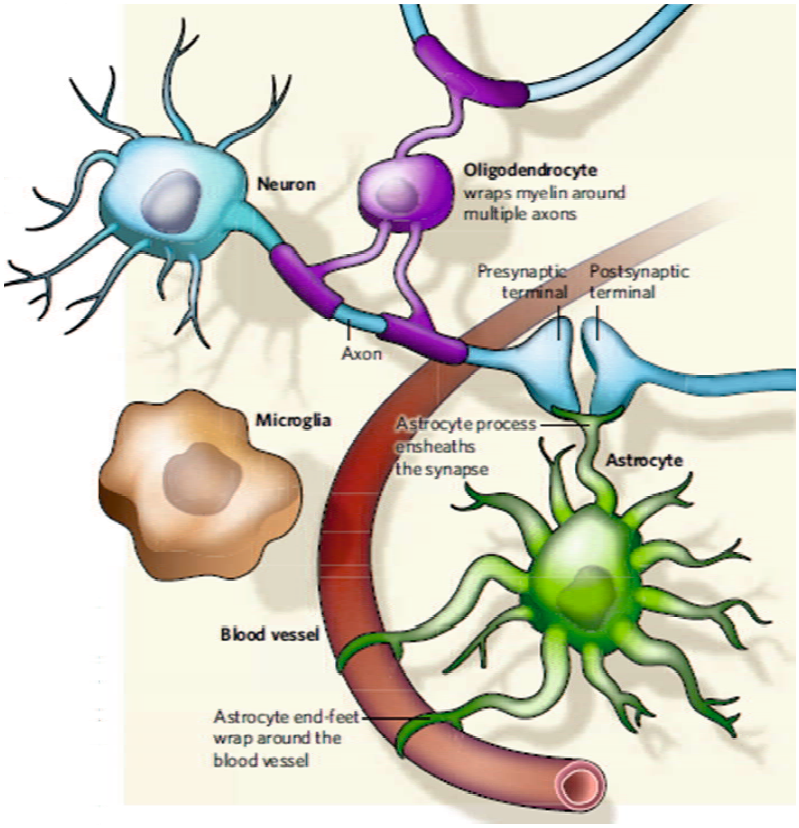

Fig. 1.1 Glial cells in the CNS and their interactions with surrounding cells. Scheme shows different types of glial cells interact with neurons and surrounding blood vessels. Oligodendrocytes enwrap myelin around axons to accelerate neuronal transmission. Astrocytes extend processes that ensheathe synapses and blood vessels. Microglia keep the brain under surveillance for damage or infection [figure taken from (1)].

Astrocytes also have pivotal influences on structural and synaptic plasticity of neurons directly through physical contact or indirectly by releasing humoral factors, such as growth factors, thrombospondins, and cholesterol (8-11). Therefore, even subtle functional impairment

of astrocytes could ultimately compromise neuronal responses and be associated with pathology of neurological disorders.

1.3. Astrocytes dysfunction and disease

Based on importance of astrocytes in normal brain function and their involvement in several activities there is no CNS disease that does not substantively involve astrocytes. Indeed, defects in the regulatory roles of astrocytes are major contributors in the pathophysiology of neurodevelopmental and neuropsychiatric disorders (12-14).

Astrocytes involved in several neurodegenerative diseases including Alzheimer´s disease (AD), Parkinson´s disease (PD), amyotrophic lateral sclerosis (ALS), and multiple sclerosis (MS) in both exacerbation of damage and neuroprotective mechanisms; and in these disorders abundant evidence is already revealed that astrocytic abnormalities and physiological dysfunction occur before onset of clinical symptoms (15).

Moreover, detailed analyses of neurodevelopmental disorders are revealed that dysfunction of astrocytes during development can be an important etiological factor in the pathology of diseases including Rett syndrome, fragile X mental retardation, Alexander's disease, and autism. Strikingly, astrocyte dysfunction has profound noncell-autonomous effects on their nearby neurons (16).

Astrocytes dysfunction have also been linked to the pathology of several neuropsychiatric disorders including major and bipolar depression, schizophrenia, and addiction (17). Therefore, understanding precise role of astrocytes in neurological and neuropsychiatric disorders requires further knowledge regarding to the biology, function, and especially their communications with surrounding neurons.

1.4. Fatty acid binding proteins (FABPs), a family of intracellular chaperons for lipophilic molecules

FABPs are low molecular weight (~15 kDa) proteins which serve as cellular chaperons for lipophilic molecules as well as fatty acids (FAs) in a large verity of cells and organs with a spatiotemporal expression pattern (18). Besides FABPs contribution to govern uptake and intracellular distribution of FAs such as arachidonic acid (AA) and docosahexaenoic acid (DHA), they are thought to be involved in metabolism, signal transduction and gene regulating activities [**Fig. 1.2**; (19-22)].

The gene regulating activity of FABPs are thought to be done by their translocation to nucleus and thereby targeting ligands (FAs) to the nuclear receptors including peroxisome proliferator activated receptors (PPARs) and retinoid X receptors (RXR) (23-25). Consistently, body of evidence regarding to physical interaction of PPARs with some FABPs proposed them as PPARs co-activators [**Fig. 1.2**; (25, 26)].

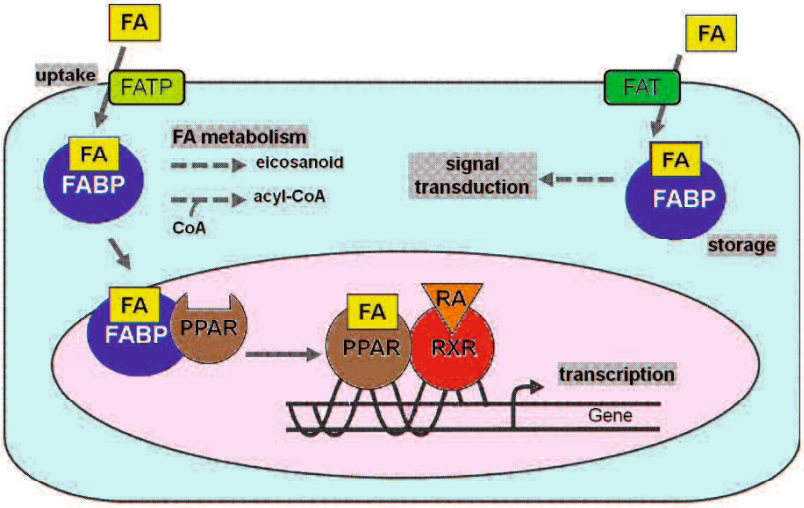

Fig. 1.2 Cellular functions of FABPs. Simplified scheme shows cellular functions of FABPs. The uptake of FAs is facilitated by membrane associated proteins as well as fatty acid transport

protein (FATP) and fatty acid translocase (FAT; CD36). Intracellular FAs are bound to FABPs, and FABP modulates several cellular procedures including synthesis of acyl-CoA and/or eicosanoids, FA-mediated signal transduction, and gene transcription by nuclear receptors like PPARs and RXR; RA: retinoic acid [figure taken from (20), with modifications].

So far at least nine members of FABP family have been recognized in mammalian species among them, FABP3 (heart-type FABP), FABP5 (epidermal-type FABP) and FABP7 (brain-type FABP) have been identified to be expressed in the brain [**Fig. 1.3**; (27-29)]. While FABP3 expression in brain is just confined to neurons, FABP5 and 7 are showing a broader expression pattern and have been shown to be expressed in neural stem cells (NSCs) and glial cells (19, 30-34).

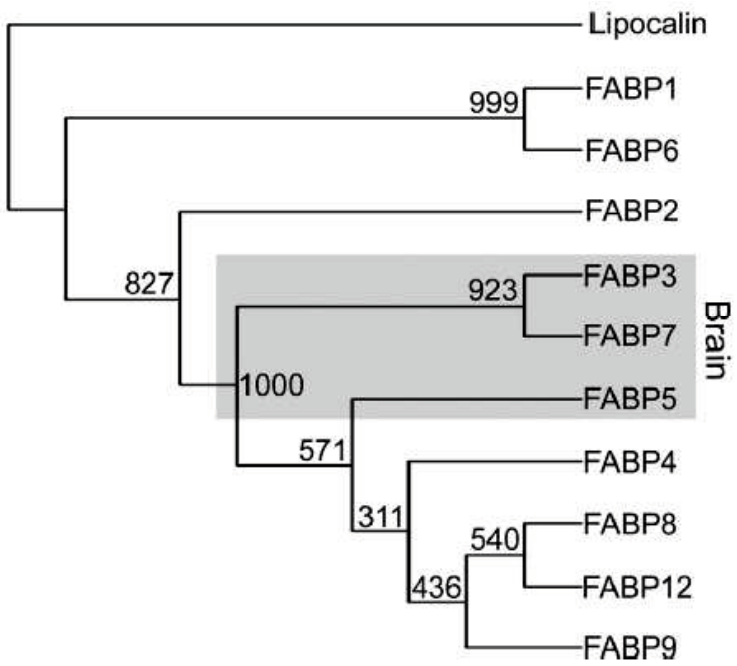

Fig. 1.3 Phylogenetic tree of fatty acid binding protein members of human. The bootstrap neighbor-joining phylogenetic tree was constructed using *CLUSTALX*. The human lipoclalin1 protein sequence (LCN1; NP_002288) was used as an outgroup. The bootstrap values (based on

number per 1000 replicates) are indicated on each node. The three phylogenetically-related FABPs with brain functions are highlighted [figure taken from (29)].

1.5. FABP7, a glia-expressed FABP

FABP7, which is preferentially bound to n-3 polyunsaturated fatty acids (PUFAs), was initially found to be expressed in neural stem cells and radial glia of the developing brain (19, 30, 35) and to be essential for neurogenesis as a positive regulator of proliferation in neural stem progenitor cells (36). In the embryonic brain, FABP7 is essential for maintenance and proliferation of neural stem progenitor cells, and *Fabp7* gene expression is downstream of Pax6 and Notch signaling (37, 38). In the adult brain, FABP7 is expressed by astrocytes and oligodendrocyte progenitor cells, whereas it is not detected in neurons, microglia, and mature oligodendrocytes (33, 34). FABP7 is reportedly enriched within synaptoneurosomal fractions from mouse brain, and its presence exhibits circadian variations, implicating a role for FABP7 in the formation of complex behavioral processes (39, 40). Augmented levels of FABP7 are also detected in the fine astrocytic perisynaptic compartments near synapses, suggesting its role in the control of neuronal activation or synaptic homeostasis (40). Although these findings have introduced FABP7 as an important biological regulator for glial cells, several aspects of this contribution remain unknown.

Our recent studies connected FABP7 to neuropsychiatric diseases (31, 41). The *Fabp7* gene is mapped to a quantitative trait locus for deficiency in prepulse inhibition, an endophenotype of schizophrenia, and *FABP7* mRNA levels are upregulated in the dorsolateral PFC of patients with schizophrenia (41). Mice with a *Fabp7* knockout (*Fabp7* KO) exhibit decreased prepulse inhibition and altered emotional behaviors (31, 41, 42). Genetic variants of *FABP7* show significant associations with neuropsychiatric diseases (41, 42). Accordingly, it is

highly possible that the expression of FABP7 in astrocytes is essential for normal neuronal structure and function, and that impairment in FABP7 causes behavioral phenotypes in FABP7-deficient mice, which can be used as a model of schizophrenia.

1.6. Neuronal morphology and dendritic structures

Dendrites are the major sites for information input into neurons and dendritic branching pattern (dendritic arbor) varies to a great extent with the neuronal type. In fact the dendritic arborization is an important determinant of the synaptic or sensory input received by a neuron (43). Several neurological disorders are linked with abnormalities in the dendritic arborization, including neurodegenerative diseases, mental retardation syndromes (such as Down's syndrome, Rett syndrome and fragile X syndrome, and neuropsychiatric disorders like schizophrenia (44-46).

Neuronal dendritic development is a complex process which should be highly coordinated at the molecular level. Recently it has been shown that a complicated interacting network of several molecules involved in signal transduction, macromolecule synthesis, cytoskeleton rearrangements and intracellular trafficking of proteins and membranes are engaged in this process. These processes are regulated by both an intrinsic ability of neurons by their genetic programs and a wide variety of extracellular signals, and astrocytes provide a number of such external cues engaged in the formation and maturation of dendritic arbor [**Fig. 1.4** (47)].

The dendrites of many neurons have numerous small protrusions (usually no longer than 2 μm) known as dendritic spines, which are often ending in a bulbous head attached to dendrite by a narrow neck (46, 48). Generally, dendritic spines are actin rich structures and consist of membrane compartments for protein synthesis and processing. In the mammalian CNS dendritic spines are the sites for more than 90% of excitatory synapses and contain post synaptic signaling complexes for excitatory synaptic transmission as well as postsynaptic density (PSD) (48, 49).

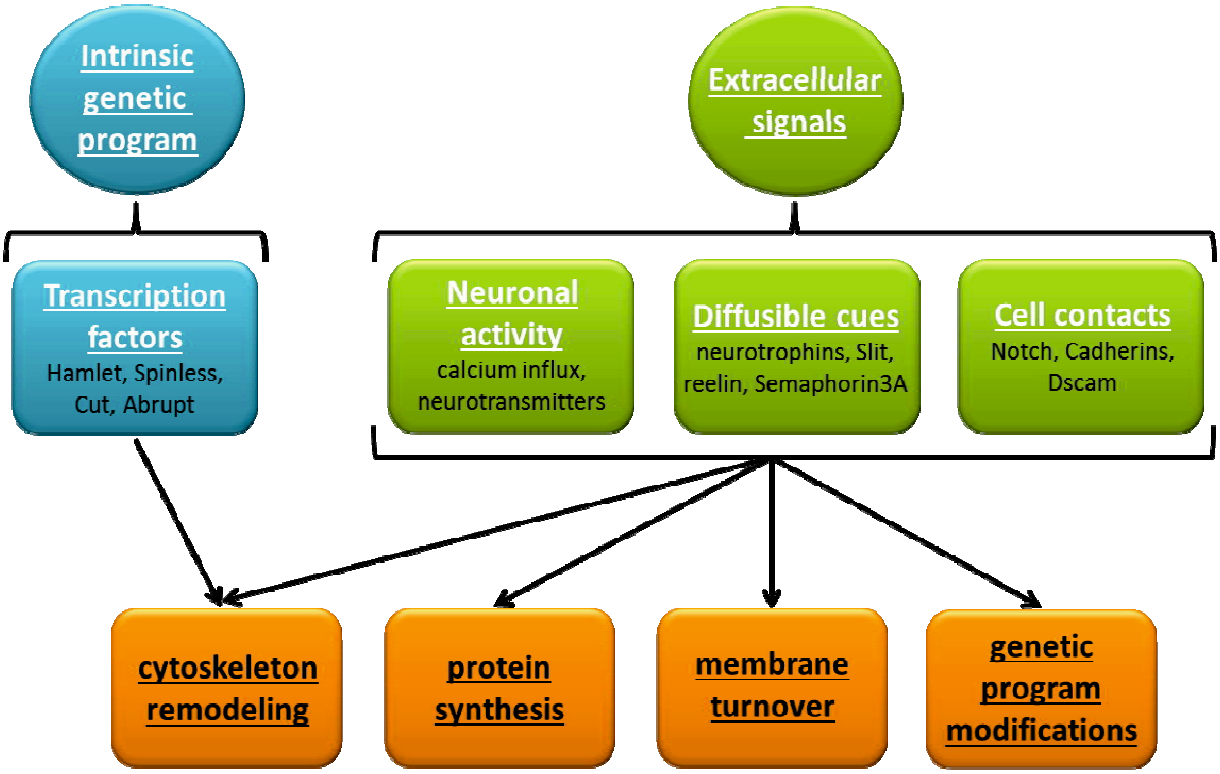

Fig. 1.4 Several overlapping processes towards development of dendritic arbor. Dendrite formation is a process regulated by combination of neuronal intrinsic genetic programs and extracellular signals triggering changes in cytoskeleton, macromolecule synthesis and membrane turnover [scheme prepared based on (43)].

Therefore, because neuronal dendrites and their dendritic spines are the principle components for synaptic formation/transmission, alterations in formation of dendritic arbor and dendritic structures are contributed to several neuropsychiatric disorders (50).

1.7. Altered neuronal morphology in neurological disorders

Neuronal dendrites and their dendritic spines are the principle components for synaptic transmission, and alterations in dendritic formation contribute to neuropsychiatric disorders (50). The prefrontal cortex (PFC) is associated with higher-order cognitive and emotional functions (51). In particular, a reduction in the complexity of dendritic branches and spine density of

pyramidal neurons in the human dorsolateral PFC, which is considered the homolog of the mouse medial PFC (mPFC), has been attributed to the pathology of neuropsychiatric disorders, including schizophrenia and autism (52, 53). However, the mechanisms underlying the regulation of synaptic formation and activity in this cortical region remain unknown.

1.8. Aim of present study

The exact functions of FABPs in different cells and organs are still poorly understood. However, development of FABPs transgenic mice and new techniques have somehow facilitated study on their roles which are leading to increase our knowledge about importance of these molecules in normal and pathological conditions and attracted further attention to their therapeutic potentials (22).

FABP7 is known to be expressed in brain and it seems that FABP7 is the most specific member of FABP family in brain. Several studies in recent years have provided evidence regarding to importance of FABP7 in the normal brain function and its implication for neurological disorders, especially neuropsychiatric disorders and gliomas. Accordingly, in this study I hypothesized that expression of FABP7 in astrocytes is essential for normal neuronal structure and function, and that impairment in FABP7 causes behavioral phenotypes in FABP7-deficient mice, which can be used as a model of schizophrenia.

The aim of this research was to explore whether the alteration in the behavioral phenotypes of *Fabp7* KO mice are associated with impairments of neuronal dendritic arborization and synaptic activity, I examined dendritic morphology, synapse formation, and basal synaptic activity in *Fabp7* KO mice and the impact of a FABP7 deficiency in astrocytes on neuronal development *in vitro* using primary cortical neuronal culture systems. Through my work, described in this section of the present thesis, I hoped to provide new insights linking

FABP7, lipid homeostasis, and neuropsychiatric disorders, which may lead to novel therapeutic interventions for such disorders.

To further explore the regulatory roles of FABP7 in astrocytes, I also needed to test the possible impacts of FABP7 deficiency on astrocyte proteome. Looking for a proof about the hypothetic influence of FABP7 on astrocyte proteomic signature; in this study I also compared the proteome of cultured astrocytes from FABP7-deficient and wild-type (WT) mice using two-dimensional gel electrophoresis (2-DE) followed by liquid chromatography mass spectrometry (LC-MS) and finally confirmed the results by Western blotting.

2. MATERIALS AND METHODS

2.1. Animals

Ten-week-old (postnatal day 70, P70) male *Fabp7* KO mice (31) and their C57BL/6 wild-type (WT) littermates were utilized for Golgi staining, immunohistochemical analyses and behavioral tests. For cell culture experiments, embryonic day 17 (E17) embryos and newborn mice (P0-P1) from both genotypes were used. For astrocyte transplantation experiments, green fluorescent protein (GFP)-expressing mice (under the control of a chicken beta-actin promoter and cytomegalovirus enhancer; C57BL/6-Tg[CAG-EGFP]) were used (54). To establish *Fabp7* KO mice with GFP expression, *Fabp7* KO mice were crossed with C57BL/6-Tg(CAG-EGFP) mice to produce heterozygous offspring. Subsequently, heterozygote mice were intercrossed, and *Fabp7* KO(CAG-EGFP) mice were identified by genotyping (data not shown). Mice were maintained under a 12 h light:dark cycle (lights on at 8:00 am) with ad libitum access to food and water.

All experimental protocols were reviewed by the Ethics Committee for Animal Experimentation of Yamaguchi University School of Medicine and were performed according to the Guidelines for Animal Experimentation of the Yamaguchi University School of Medicine under the laws and notification requirements of the Japanese Government.

2.2. Neuron-enriched primary mixed cortical cultures

Neuron-enriched primary mixed cortical cultures were prepared from cerebral cortices of newborn *Fabp7* KO and WT mice (P0-P1) as previously described (55) with some modifications [**Fig. 2.1**]. Briefly, mouse cortical cells were dissociated by papain (90 units/ml; Worthington

Biochemicals, Lakewood, NJ, USA) treatment at 37 °C for 15 min with gentle shaking, followed by trituration with a plastic serological pipette (Greiner Bio-One, Frickenhausen, Germany). Isolated cells were seeded onto 35-mm culture dishes (Becton Dickinson Labware, Franklin Lakes, NJ, USA) coated with polyethyleneimine (Wako Pure Chemical Industries, Osaka, Japan) at a final seeding density of 2.5×10^5 cells/ml. The culture medium consisted of DMEM-F12 (GIBCO, Grand Island, NY, USA) supplemented with 5% heat-inactivated fetal bovine serum (FBS; HyClone; Thermo Scientific, Waltham, MA, USA), 5% heat-inactivated horse serum (HS; Invitrogen, Carlsbad, CA, USA), and 1% penicillin-streptomycin (Sigma-Aldrich, St. Louis, MO, USA). The cortical cultures were grown for 7 days in vitro (DIV-7) and then assessed for neuronal dendritic morphology using immunocytochemistry. In total, three independent cortical cultures (at least three dishes per genotype per culture) were used.

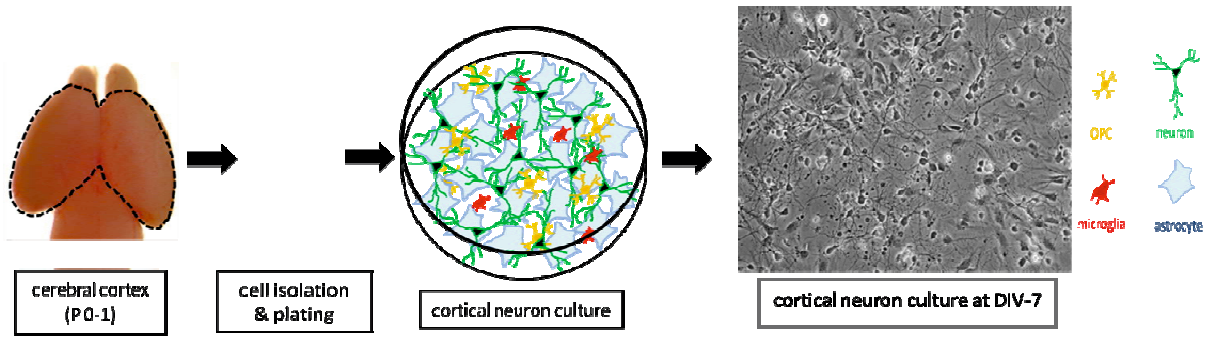

Fig. 2.1 Neuron-enriched primary mixed cortical culture. Scheme shows cortical neuron culture. *Fabp7* KO and WT postnatal day 0-1 were used for this culture system, morphological assessments were performed at DIV-7.

The survival of cortical neurons in primary mixed cortical cultures was evaluated as previously described (56). Briefly, cell survival was measured by counting the number of neurons observed in phase contrast microscopic images captured from pre-marked microscopic fields (1 mm^2), 1 day after plating and at DIV-7. The percentage of viable neurons was

calculated based on the number of neurons surviving at DIV-7. Three independent cultures from each genotype were examined (at least three dishes per genotype per experiment).

2.3. Primary cortical neuron-astrocyte co-cultures

Primary dissociated neuron-astrocyte co-cultures were prepared as previously described (57). Briefly, to prepare astrocytic cultures, cerebral cortices from *Fabp7* KO and WT mice (P0-P1) were sampled and dissociated by trypsin treatment (0.25%; Invitrogen) at 37 °C for 15 min followed by trituration with a serological plastic pipette (Greiner Bio-One). Harvested cells from three cortical hemispheres were seeded onto a T75 culture flask (Becton Dickinson Labware) in MEM (Invitrogen) supplemented with 10% HS (Invitrogen) and 0.6% glucose (Wako Pure Chemical Industries). After the cells became confluent (10-14 days), flasks were shaken on an orbital shaker (BR-40LF; TAITEC, Koshigaya, Japan) at 200 rpm for 24 h at 37 °C to eliminate other glial cells. Subsequently, astrocytes were subcultured on 12-mm glass coverslips (Matsunami, Kishiwada, Japan) coated with poly-l-lysine (1 mg/ml; Sigma-Aldrich) and laminin (0.1 mg/ml; Invitrogen) in 24-well plates (Becton Dickinson Labware) at a final seeding density of 2.5×10^4 cells/well for 8 to 10 days [**Fig. 2.2**].

To prepare primary cortical neuronal cultures, cerebral cortices from WT embryos (E17) were sampled and dissociated using trypsin (0.25%; Invitrogen) followed by trituration with a fire-polished glass Pasteur pipette. The obtained WT neurons were seeded at a density of 2×10^4 cells/well over WT or *Fabp7* KO astrocytic monolayers and grown for 7 days in serum-free medium consisting of MEM enriched with 1% N2 supplement (Invitrogen), 1 mM sodium pyruvate (Invitrogen) and 0.6% glucose (Wako Pure Chemical Industries). Quantitative immunocytochemical evaluation of neuronal morphology and synaptic protein expression was

performed. Three independent experiments (at least three coverslips per genotype per experiment) were performed [**Fig. 2.2**].

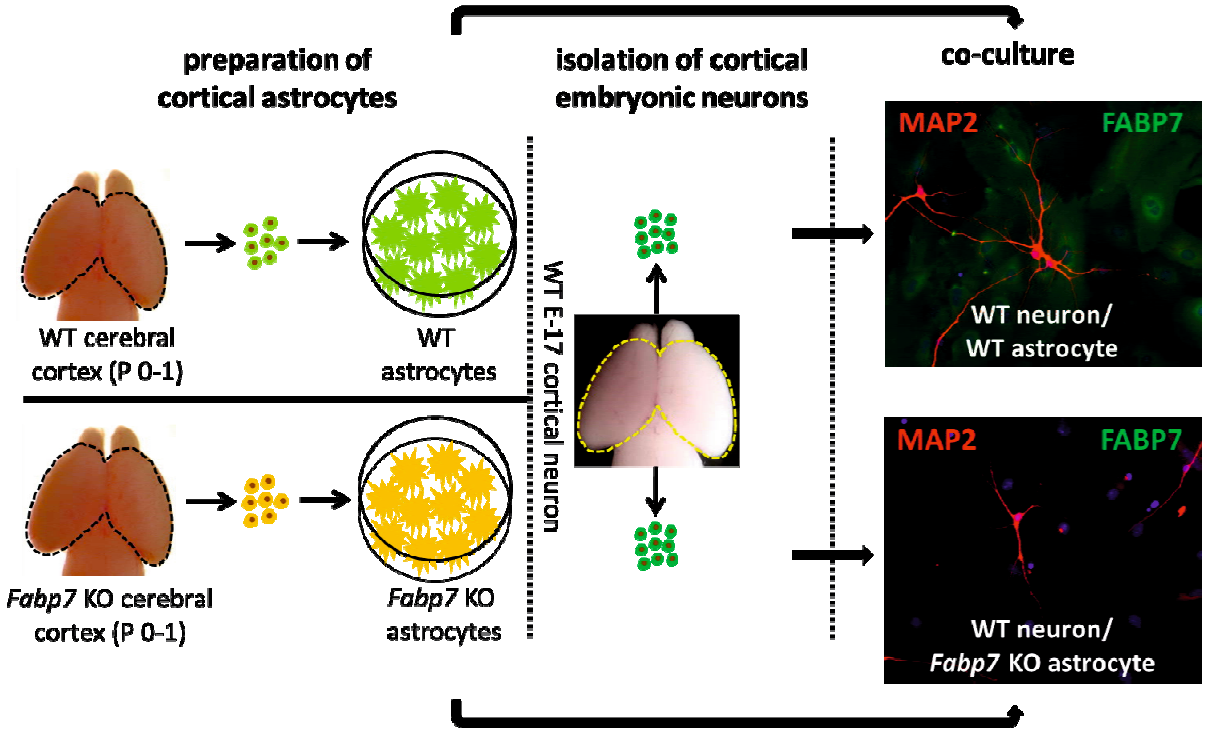

Fig. 2.2 Primary cortical neuron-astrocyte co-culture. Scheme shows cortical neuron/ astrocyte hybrid co-culture. WT embryonic (E17) neurons were co-cultured for 7 days with primary cortical astrocytes from either WT or FABP7-KO mice.

The population density of astrocytes was obtained using 20 random images (40× lens, image area 0.05 mm^2) from each coverslip under a fluorescence microscope (AxioObserver; Carl Zeiss, Oberkochen, Germany). The population density of astrocytes in WT and *Fabp7* KO co-cultures was evaluated by counting those nuclei stained with 4',6-diamidino-2-phenylindole (DAPI, 0.5 µg/ml; Invitrogen) in each microscopic field. Astrocytes were identified by their large bean-shaped nuclei containing several nucleoli, and neurons were identified by their smaller and compact round-shaped nuclei (58). For quantitative analyses, three independent

cortical neuron-astrocyte co-cultures with either *Fabp7* KO or WT astrocytes were examined (at least three coverslips per condition per independent culture).

2.4. Preparation of astrocyte-conditioned medium (ACM) and cortical neuronal cultures with ACM

For ACM preparation, astrocytic cultures were established from cerebral cortices of newborn mice (*Fabp7* KO and WT) as described above. After shaking, astrocytes were passaged and seeded in 60-mm culture dishes (Becton Dickinson Labware) at a density of 1.5×10^5 cells/ml and maintained until the cultures became confluent (approximately 7 days). After reaching confluency, the cells were thoroughly washed with D-PBS (Nissui Pharmaceutical, Tokyo, Japan), and the medium was changed to DMEM-F12 (GIBCO) without serum for conditioning. The ACM was collected 24 h later, passed through 0.2-μm filters (Minisart; Sartorius, Gottingen, Germany) to remove debris and applied to the cortical neuronal cultures. After obtaining ACM, the population density of astrocytes was examined under phase contrast imaging, and no significant difference was detected between the two genotypes (data not shown).

In this experiment, WT cortical neurons (E17; 5×10^4 cells) were seeded onto 12-mm glass coverslips (Matsunami) coated with poly-l-lysine (1 mg/ml; Sigma) in neuronal plating medium consisting of DMEM-F12 (GIBCO) supplemented with 5% FBS (HyClone; Thermo Scientific), 5% HS (Invitrogen), and 1% penicillin-streptomycin (Sigma-Aldrich). After 4-5 h of incubation for optimal attachment of neural cells, the neuronal plating medium was replaced with neural maintenance medium, consisting of DMEM-F12 (GIBCO) enriched with 2% B27 supplement (Invitrogen), 1 mM sodium pyruvate (Invitrogen), and 1% penicillin-streptomycin (Sigma-Aldrich). Three days after plating, the neural maintenance medium was replaced with freshly prepared ACM (*Fabp7* KO and WT) enriched with 2% B27 supplement (Invitrogen)

after first thoroughly rinsing with D-PBS (Nissui Pharmaceutical). To inhibit glial cell proliferation, cytosine arabinoside (AraC; Sigma-Aldrich) was added to the neuronal culture medium at a final concentration of 5 μM. One-third of the culture medium was replaced with fresh ACM every 3 days, and the immunocytochemical morphometric investigation of neurons was conducted after 7 days [**Fig. 2.3**].

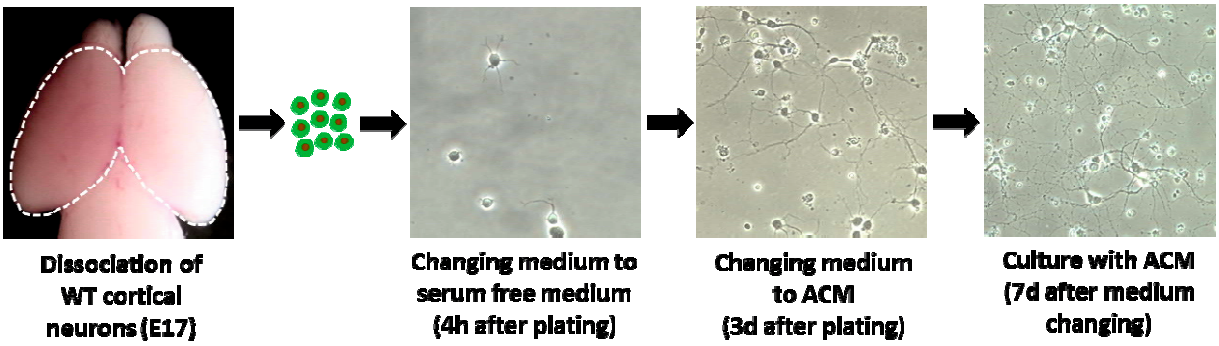

Fig. 2.3 Scheme shows preparation of cortical neuronal cultures with ACM.

The population density of cortical neurons was examined after 7 days of culture with ACM (WT and *Fabp7* KO). The cells were fixed with 4% PFA (Nacalai Tesque, Kyoto, Japan) and immunostained with a microtubule-associated protein 2 (MAP2) antibody (immunocytochemistry is described in detail in the following sections). From each coverslip, five random images were captured using a fluorescence microscope (20× lens; Zeiss; image area 0.2 mm^2). The population density was evaluated by counting MAP2-positive ($MAP2^+$) cells in each microscopic field. Three independent cortical neuron cultures with either *Fabp7* KO or WT ACM were evaluated (at least three coverslips per condition per independent culture).

2.5. Immunohistochemistry

Immunohistochemistry was performed as described previously (33, 34). Briefly, mice (P70) were transcardially perfused with freshly prepared 4% PFA (Nacalai Tesque) in 0.1 M sodium

phosphate buffer (pH 7.4), and the brains were postfixed in 4% PFA overnight at 4 °C. After cryoprotection in graded concentrations of sucrose (Wako Pure Chemical Industries; 10%, 20%, and 30%) in PBS, coronal sections containing mPFC (bregma +2.4 mm to +1.5 mm) were sliced at 14 μm thick using a cryostat (CM1850; Leica, Nussloch, Germany) in accordance with a mouse brain atlas (59). Brain sections were permeabilized with 0.3% Triton X-100 (Sigma-Aldrich) in PBS, blocked with 5% skim milk in T-PBS, and incubated overnight at 4 °C with a combination of specific primary antibodies, including chicken anti-MAP2 (1:10,000; Neuromics, Edina, MN, USA), rabbit anti-FABP7 (0.5 μg/ml) (31), rat anti-CD11b (1:50; Chemicon Temecula, CA, USA), rat anti-GFAP (1:200; Invitrogen), rat anti-PDGFRα (1:500; eBioscience, San Diego, CA), mouse anti-NeuN (1:100; Millipore, Billerica, MA, USA), and mouse anti-OLIG2 (1:500; Millipore) [**Table 2.1**]. The sections were then incubated with a combination of Alexa-conjugated secondary antibodies (goat anti-chicken IgG-Alexa 594, goat anti-rabbit IgG-Alexa 488 or IgG-Alexa 568, goat anti-rat IgG-Alexa 488 or IgG-Alexa 568, and goat anti-mouse IgG-Alexa 488 or IgG-Alexa 568; Invitrogen). After nuclear staining with DAPI (0.5 μg/ml; Invitrogen), slides were coverslipped using Fluoromount (Diagnostic BioSystems, Pleasanton, CA, USA).

To evaluate the population density of different neural cell types in the mPFC, images (four sections per animal, six images per section) were captured and processed with a confocal laser scanning microscope (LSM510 META; Carl Zeiss) using a 40× lens (digital zoom 0.8, image area 0.08 mm^2) and ZEN 2011 imaging software (Carl Zeiss), respectively. The population densities of $NeuN^+$ neurons (WT = 94 images and *Fabp7* KO = 98 images), $GFAP^+$ astrocytes (WT = 93 images and *Fabp7* KO = 94 images), and $OLIG2^+$ oligodendrocyte lineage

cells (WT = 94 images and *Fabp7* KO = 95 images) were compared between *Fabp7* KO and WT mice.

Table 2.1 Information of primary antibodies utilized in this study.

antibody	host species	dilution rate	vendor/reference	target (cells)
anti-CD11b	rat	1:50	Chemicon	microglia
anti-FABP7	rabbit	0.5 μg/ml (0.125 μg/ml for WB)	Owada et al., 2006	
anti-GFAP	rat	1:200 (1:2500 for WB)	Invitrogen	astrocyte
anti-MAP2	chicken	1:10,000	Neuromics	neuron (somatodendritic marker)
anti-NeuN	mouse	1:100	Millipore	neuron (nucleus marker)
anti-OLIG2	mouse	1:500	Millipore	whole oligodendrocyte lineage cells
anti-PDGFRα	rat	1:500	eBioscience	oligodendrocyte progenitor cell (OPC)
anti-PSD95	rabbit	1:250	Invitrogen	synaptic density protein 95 (postsynaptic marker of excitatory synapse)
anti-synaptophysin	mouse	1:250	Sigma-Aldrich	major synaptic vesicle protein (presynaptic marker of excitatory synapse)
anti-VGlut1	guinea pig	1:1000	Millipore	vesicular glutamate transporter 1 (presynaptic marker of excitatory synapse)
anti- PEA-15	rabbit	1:500	Santa Cruz Biotech	
anti- vimentin	mouse	1:500	Abcam	
anti-β-actin	mouse	1:5000	Santa Cruz Biotech	

2.6. Golgi staining and *in vivo* assessment of neuronal morphology

Golgi staining was performed using a Rapid GolgiStain kit according to the manufacturer's protocol (FD NeuroTechnologies, Columbia, MD, USA). Briefly, brains of *Fabp7* KO mice and their WT littermates (five mice per genotype, P70) were immediately removed after cervical dislocation, and the dissected brains were immersed in impregnation solutions (solutions A and B) for two weeks, cryoprotected (solution C) for three days at 4 °C, and then snap frozen and stored at -80 °C. The brain samples were coronally sectioned at a thickness of 120 μm using a

cryostat (CM1850; Leica) and mounted on 1% gelatin-coated glass slides [**Fig. 2.4**]. The sections were then stained with the staining solution (solutions D and E) and coverslipped using Permount (Fisher Scientific, Houston, TX, USA).

To assess dendritic morphology, low magnification (20× lens) images (Z-stack with 1 µm intervals) of pyramidal neurons, with cell bodies located in layer II/III of mPFC [**Fig. 2.4**], were randomly captured using a confocal laser scanning microscope (LSM510 META; Carl Zeiss). All captured images from Sholl analysis *Fabp7* KO (n = 41 neurons) and WT brains (n = 39 neurons) were manually traced using Neurolucida software (MBF Biosciences, Williston, VT, USA). For traced neurons, the total dendritic length, number of dendritic branches, and area covered by the dendritic tree were measured with Neurolucida Explorer software (MBF Biosciences). The complexity of the dendritic trees from the apical and basal dendrites was also evaluated using Neurolucida Explorer software.

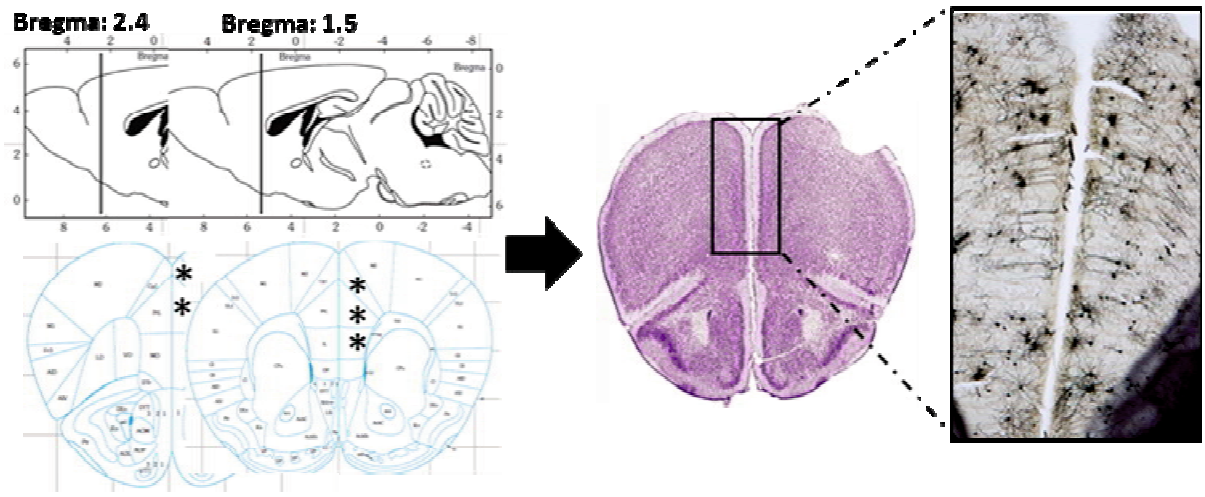

Fig. 2.4 Location of mPFC in the mouse brain [cartoons and Nissl staining image taken from (59)] and representative image of Golgi staining of mPFC in the mouse brain.

To assess dendritic spine morphology, high magnification (63× lens and digital zoom 3) images (Z-stack with 0.33 µm intervals) of the pyramidal neurons described above were captured.

The density of the dendritic spines was quantified by counting the number of spines on the following segments: dendritic segments (50-100 μm) of the apical dendrites located farther than 50 μm from the cell soma of *Fabp7* KO (n = 39 dendrites) and WT (n = 43 dendrites) pyramidal neurons; dendritic segments (50-100 μm) of basal dendrites located farther than 20 μm from the cell soma of *Fabp7* KO (n = 40 dendrites) and WT (n = 39 dendrites) pyramidal neurons. The morphology of the dendritic spines was classified based on their morphological appearance as described elsewhere (60). An investigator who was blinded to the genotype of samples performed the assessments using Neurolucida Explorer software (MBF Biosciences).

2.7. Immunocytochemistry and assessment of neuronal morphology

For the immunocytochemical study, the cultured samples were fixed using 4% PFA (Nacalai Tesque) in phosphate buffer for 15 min, and then washed three times with cold D-PBS (Nissui Pharmaceutical). The blocking procedure was performed with a solution containing 10% HS and 0.2% Triton X-100 (Sigma-Aldrich) in D-PBS (Nissui Pharmaceutical). The immunostaining was performed by incubating samples with specific primary antibodies overnight at 4 °C **[Table 2.1]**. The following primary antibodies diluted in the blocking solution were applied: chicken anti-MAP2 (1:10,000; Neuromics), rat anti-GFAP (1:200, Invitrogen), and rabbit anti-FABP7 (0.5 μg/ml) (31). Following the primary antibody incubations, samples were washed three times with D-PBS (Nissui Pharmaceutical) and incubated for 1 h with a combination of Alexa-conjugated secondary antibodies (goat anti-chicken IgG-Alexa 594; goat anti-mouse IgG-Alexa 488 or IgG-Alexa 568; goat anti-rat IgG-Alexa 488 or IgG-Alexa 568, and goat anti-rabbit IgG-Alexa 488 or IgG-Alexa 568; Invitrogen) diluted to a ratio of 1:1000 in the blocking solution. DAPI was added (0.5 μg/ml; Invitrogen) as a nuclear stain, and samples were coverslipped using Fluoromount (Diagnostic BioSystems).

To evaluate the morphology of the cultured neurons described above, more than 20 $MAP2^+$ neurons (per coverslip or culture dish) were randomly imaged using a fluorescence microscope (AxioObserver; Carl Zeiss) with AxioVision image acquisition software (Rel4.8; Carl Zeiss). A plug-in written for ImageJ (NIH), NeuronMetrics (http://www.ibridgenetwork.org/arizona/; UA07-56-Neuronmetrics) (61), was used to evaluate the number of dendritic branches, total length of dendritic branches and the area covered by the dendritic arbor [**Fig. 2.5**].

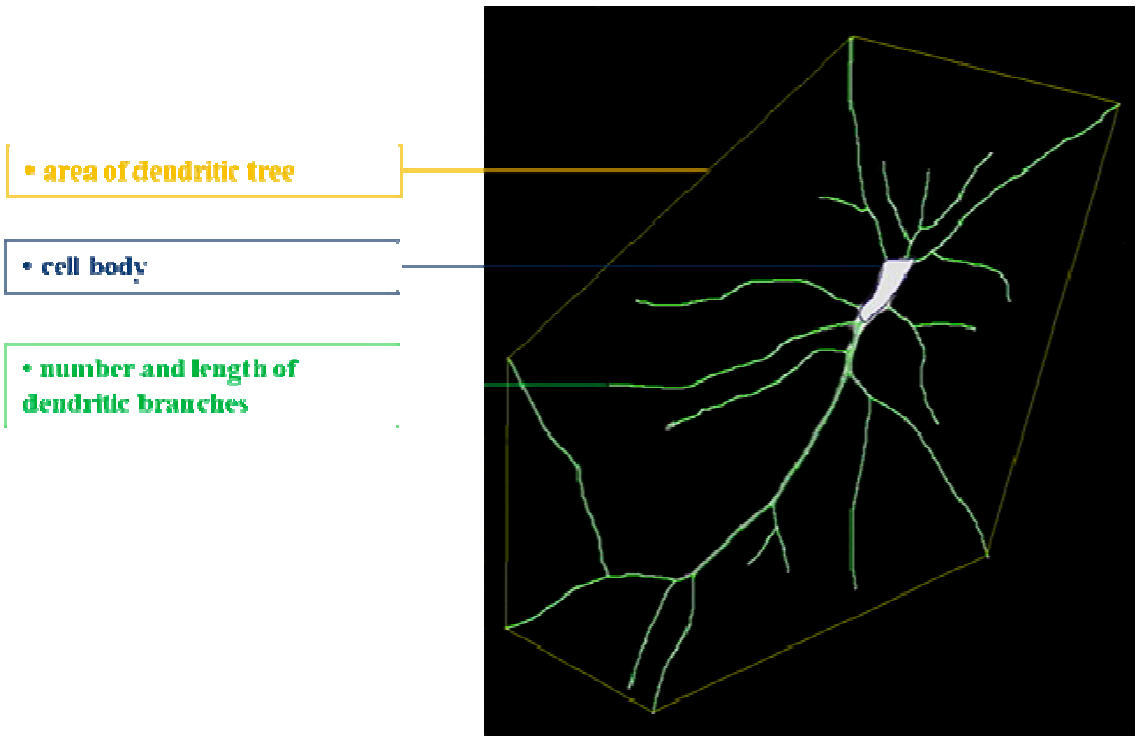

Fig. 2.5 Neuronal morphological parameters evaluated using NeuronMetrics. Immunofluorescence micrograph representing a cortical neuron stained with the MAP2 antibody and overlaid with skeletons generated by NeuronMetrics software showing the parameters measured to evaluate neuronal morphological characteristics.

2.8. Quantification of synapse number

The number of excitatory synapses in the mPFC of mice was quantified using an immunohistochemical-based method described elsewhere with slight modifications (62, 63). Briefly, *Fabp7* KO mice and their WT littermates were used for *in vivo* synapse quantification (four mice per genotype, P70). After perfusion with sufficient PBS to remove the blood from the capillaries, brains were immersed in freshly prepared 4% PFA (Nacalai Tesque) at 4 °C overnight for fixation. Subsequently, the samples were cryoprotected in 30% sucrose (Wako Pure Chemical Industries) in PBS. Coronal sections containing mPFC (at least three sections per brain) at a thickness of 14 μm were cut using a cryostat (CM1850; Leica). The sections were dried at room temperature for less than 30 min, and after a brief wash in PBS, they were blocked with 20% normal goat serum (Invitrogen) in PBS for 1 h. The sections were incubated in a PBS solution containing 10% normal goat serum and 0.3% Triton X-100 (Sigma-Aldrich) with a combination of specific primary antibodies against presynaptic protein VGlut1 (guinea pig; 1:1000; Millipore) and postsynaptic protein PSD95 (rabbit; 1:250; Invitrogen) overnight at 4 °C [**Table 2.1**]. After incubation with primary antibodies, the sections were incubated for 2 h with a combination of Alexa-conjugated secondary antibodies (goat anti-rabbit IgG-Alexa 488 and goat anti-guinea pig IgG-Alexa 555; Invitrogen) diluted at 1:1000 in the same solution as that used for primary antibodies. DAPI (0.5 μg/ml; Invitrogen) was added as a nuclear stain, and slides were coverslipped using Fluoromount (Diagnostic BioSystems).

Using a confocal laser scanning microscope (LSM510 META; Carl Zeiss), images of mPFC layer II/III were obtained (six images per section). Briefly, a 9 μm confocal scan was performed with an optical thickness of 0.33 μm (28 optical slices per image) using a 63× lens (scanned area 0.02 mm^2). The maximum intensity projections (MIP) of the consecutive optical slices were analyzed using Puncta Analyzer, a plug-in written for ImageJ (NIH, ver. 1.26; written

by Bary Wark; kindly provided by Dr. Cagla Eroglu, Department of Cell Biology, Duke University Medical Center, Durham, North Carolina) for counting co-localized pre- and postsynaptic markers (puncta). Based on the analysis of co-localized pre- and postsynaptic puncta, the number of excitatory synapses was calculated and compared between *Fabp7* KO and WT mice (more than 50 images each for WT and *Fabp7* KO mice).

The number of excitatory synapses in the cortical neurons co-cultured with either *Fabp7* KO or WT cortical astrocytes was quantified utilizing an immunocytochemical-based method as previously described (62). Briefly, after incubations with primary antibodies against the presynaptic proteins synaptophysin (mouse; 1:250; Sigma-Aldrich) and PSD95 (rabbit; 1:250; Invitrogen) [**Table 2.1**], the cells were incubated with a combination of Alexa-conjugated secondary antibodies (goat anti-rabbit IgG-Alexa 488 and goat anti-mouse IgG-Alexa 568; Invitrogen). DAPI (0.5 μg/ml; Invitrogen) was added as a nuclear dye, and coverslips were mounted on glass slides using Fluoromount (Diagnostic BioSystems).

To quantify the number of excitatory synapses, isolated neurons were randomly selected based on DAPI staining, and images were captured on all channels. To avoid bias, an investigator blind to the identity of samples randomly chose neurons from coded slides. Three dendritic segments farther than 20 μm from the cell soma were imaged from 20 neurons selected from each independent culture (three independent cultures) using a 63× lens on a fluorescence microscope (AxioObserver; Carl Zeiss) and AxioVision image acquisition software (Rel4.8; Carl Zeiss). Co-localized pre- and postsynaptic puncta were considered excitatory synapses and were assessed using Puncta Analyzer. The number of co-localized puncta was calculated and the results presented as the average number of synapses per 50 μm of the dendrite for comparisons between WT cortical neurons co-cultured with *Fabp7* KO and WT cortical astrocytes.

2.9. Electrophysiology

The whole-cell patch-clamp recordings were performed on 10-week-old *Fabp7* KO male mice and age-matched WT littermates (n = 4 mice/genotype) as previously described (64). Briefly, following to deep anesthetization of animals with pentobarbital (40 mg/Kg) and perfusion with carbogenated (95% O2/5% CO2) ice-cold dissection buffer (containing: 25.0 mM $NaHCO_3$, 1.25 mM NaH_2PO_4, 2.5 mM KCl, 0.5 mM, $CaCl_2$, 7.0 mM $MgCl_2$, 25.0 mM glucose, 110.0 mM choline chloride, 11.6 mM ascorbic acid) animals were quickly decapitated, and their brains were removed. Acute coronal brain slices (350 μm) from mPFC were cut by using a vibratome (Leica VT-1200, Nussloch, Germany) in dissection buffer and transferred into carbogenated physiological solution (containing: 118 mM NaCl, 2.5 mM KCl, 26 mM $NaHCO_3$, 1 mM NaH_2PO_4, 10 mM glucose, 4 mM $MgCl_2$, 4 mM $CaCl_2$, pH 7.4) at room temperature (22–25 °C). For whole-cell patch-clamp recordings, glass recording electrodes (4-7 MΩ) were made with a horizontal puller (P97, Sutter Instrument, Novato, CA) and filled with intracellular solution (containing: 115 mM cesium methanesulfonate, 20 mM CsCl, 10 mM Hepes, 2.5 mM $MgCl_2$, 4 mM Na_2ATP, 0.4 mM Na_3GTP, 10 mM sodium phosphocreatine, 0.6 mM EGTA at pH 7.25). The recordings were made using Axopatch–1D amplifier (Axon Instruments, Foster City, CA); signals were digitized at 5 kHz by Digidata 1440 AD board (Axon Instruments) and subsequently analyzed offline with pCLAMP 10 software (Axon Instruments). The action potential-independent miniature excitatory postsynaptic currents (mEPSCs) and miniature inhibitory postsynaptic currents (mIPSCs) were obtained from the mPFC layer II/III cortical pyramidal neurons. The pyramidal neurons were identified based on their morphological characteristics under microscope. The mEPSCs (holding potential at -60 mV; n = 55 neurons from *Fabp7* KO mice and n = 56 neurons from WT mice) and mIPSCs (holding potential at 0

mV; n = 35 neurons from *Fabp7* KO mice and n = 34 neurons from WT mice) were recorded for 5 min in the presence of tetrodotoxin (TTX; 0.5 μM; Wako Pure Chemical Industries) in bath solution to block APs. Frequency and amplitude of mEPSCs and mIPSCs above 10 pA were analyzed and compared between *Fabp7* KO and WT mice.

2.10. Behavioral tests and cell transplantation

For behavioral analysis, the open field test was performed. Behavioral measurements were conducted in a dimly lit, isolated experimentation room during the first half of the dark period. For acclimation, mice were transferred in their home cages to the examination room at least 1 h prior to the onset of tests. Male P70 *Fabp7* KO (n = 18) and WT (n = 16) mice were placed in the center of a rectangular chamber (50 × 50 × 40 cm). The floor of the field, equally divided into 36 virtual squares, was made of gray plastic (Muromachi kikai, Tokyo, Japan). Each mouse was permitted to freely explore the arena for 5 min, and its exploration was recorded with a video camera connected to tracer software (Muromachi kikai). During a mouse's only experience in the field, a number of parameters, such as total distance traveled, total time traveled, and the number of crossings from one square to another was recorded, and results for *Fabp7* KO and WT mice were compared.

For transplantation studies, GFP-expressing astrocytes were prepared from newborn *Fabp7* KO(CAG-EGFP) mice and their WT(CAG-EGFP) littermates. Astrocytes were cultured as described above. Before transplantation, GFP-expressing astrocytes obtained from *Fabp7* KO or WT mice were dissociated by mild trypsinization (0.05% trypsin) and resuspended in D-PBS (Nissui Pharmaceutical) at a density of 2.5×10^4 cells/μl. The cells were stereotaxically transplanted bilaterally into the mPFC (2 mm anterior to bregma, ± 0.4 mm lateral to midline and 1.5 mm below the skull surface) of male *Fabp7* KO mice (P56). The microinjection was

manually performed using a 10 μl glass Hamilton syringe (Hamilton, Reno, NV, USA) connected to a 29 gauge needle at a rate of 1 μl/min. In total, 2 μl of the cell suspension was injected into each side of brain (5×10^4 cells/side), and after the injection, the needle remained in the injection site for an additional 5 min. For control mice, the vehicle (2 μl of D-PBS without cells) was injected into the mPFC of *Fabp7* KO mice (n = 14) following the same surgical procedure as that for the experimental groups. Two weeks after the operation, mice performed the open field test as described above, and the results were compared across experimental groups [**Fig. 2.6**].

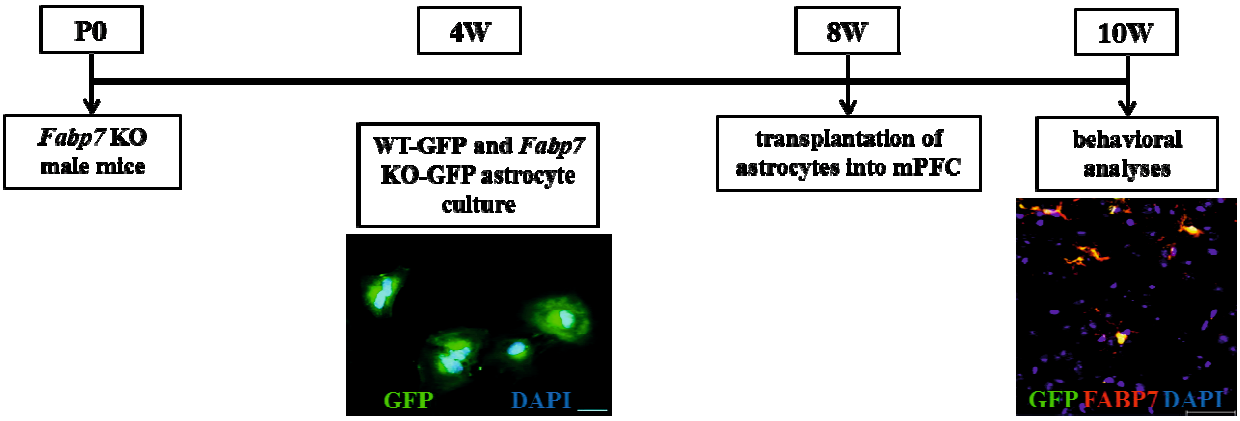

Fig. 2.6 Outline of experiment for transplantation of astrocytes into the mPFC of *Fabp7* KO mice.

After the behavioral tests, the brains of the operated mice were perfused and postfixed with 4% PFA (Nacalai Tesque), and frozen sections containing the transplantation site were prepared. The presence of GFP-expressing cells was confirmed using a fluorescence microscope (data not shown).

2. 11. Preparation of protein samples for Proteomic differential display analysis

To preparation protein samples, astrocytic cultures were established from cerebral cortices of newborn mice (*Fabp7* KO and WT) as described above. The harvested pellets from *Fabp7* KO

and WT astrocyte were homogenized in a lysis buffer containing 50 mM Tris-HCl (pH 7.5), 165 mM sodium chloride, 10 mM sodium fluoride, 1 mM sodium vanadate, 1 mM phenylmethylsulfonyl fluoride, 10 mM EDTA, 10 mg/mL aprotinin, 10 mg/ml leupeptin (all from Sigma-Aldrich), and 1% NP-40 (Nacalai Tesque) on ice. Cell suspensions were incubated for 1 h at 4 °C, centrifuged at 21,500 × g for 30 min at 4 °C, and the supernatants were stored at -80 °C till use in the next steps (65, 66).

2.12. 2-DE analysis

To perform each 2-DE, 80 micrograms of isolated protein was used. For the first dimension, isoelectric focusing (IEF) was accomplished in an IPGphor 3 IEF unit (GE Healthcare, Buckinghamshire, UK) on 11 cm, immobilized, linear gradient strips (pH 3-10; Bio-Rad, Hercules, CA, USA) at 50 μA/strip. At first protein samples were dissolved in 200 μl of rehydration buffer [consist of 8M urea (Sigma-Aldrich), 2% CHAPS (Sigma-Aldrich), 0.01% bromophenol blue (Wako Pure Chemical Industries), and 1.2% Destreak reagent (GE Healthcare)] and 0.5% IPG (immobilized pH gradient) buffer (GE Healthcare), and then loaded into the IPGphor strip holder (GE Healthcare). IEF was done according to the following voltage program: rehydration for 10 h (no voltage), 0 to 500 V for 4 h, 500 to 1000 V for 1 h, 1000 to 8000 V for 4 h, 8000 V for 20 min, and a final phase of 500 V from 20,000 to 30,000 Vh. For the second dimension the IPG strips were then transferred onto precast polyacrylamide gels with a linear concentration gradient of 5-20% (Bio-Rad) and run for 1 h at 200 V (66).

Following the 2-DE, the SDS-PAGE gels were fixed using a fixing solution consists of 40% ethanol (Wako Pure Chemical Industries) and 10% acetic acid (Wako Pure Chemical Industries) for more than 2 h. To label proteins with fluorescent dye, gels were stained with Flamingo™ Fluorescent Gel Stain (Bio-Rad) overnight (66).

2.13. Image analysis and spot picking and in gel digestion

To evaluate the protein spots, stained gels were washed with Milli-Q water three times each for 5 min and then were observed using the ProEXPRESS 2D Proteomic Imaging System (PerkinElmer, Waltham, MA, USA). The intensity of each spot was quantified with Progenesis Samespots software (Nonlinear, Newcastle, upon Tyne, UK) (67). Using five biological replicates and two technical replicates, the differences in expression levels between *Fabp7* KO and WT (astrocyte lysate) were analyzed statistically by the student's t-test. The gels were restained with See Pico^{TM} (Benebiosis, Seoul, Korea), and the selected spots with differential intensity between the two genotypes were cut and removed for the MS analysis.

To remove See Pico^{TM} dye (Benebiosis), gel pieces were washed three times in 60% methanol (Sigma-Aldrich), 50 mM ammonium bicarbonate, and 5 mM DTT (both from Wako Pure Chemical Industries) for 15 min. The sample in the gel pieces was reduced twice in 50% ACN (Sigma-Aldrich), 50 mM ammonium bicarbonate, and 5 mM DTT for 10 min. The gel pieces were dehydrated in 100% ACN twice for 30 min, and then in-gel digestion was done with a reagent containing 10 μg/ml sequencing grade-modified trypsin (Promega, Madison, WI) in 30% ACN, 50 mM ammonium bicarbonate, and 5 mM DTT. The in-gel digestion procedure was completed at 30 °C overnight. Then, digested samples were lyophilized overnight using a lyophilizer (Lyph-lock 1L Model 77400, Labconco, Kansas, MO, USA).

2.14. LC-MS/MS analysis

The lyophilized samples were dissolved in 0.1% formic acid (Sigma-Aldrich), centrifuged at 21,500 × g for 5 min, and the supernatant was used for MS analysis. Twenty-five microliters of each sample was analyzed using a LC-MS/MS system (Agilent 1100 LC-MSD Trap XCT, Agilent Technologies, Palo Alto, CA, USA). Protein identification procedure was performed

using Agilent Spectrum MILL MS proteomics workbench against the Swiss-Prot protein database search engine (http://kr.expasy.org/sprot/) and MASCOT MS/MS Ions Search engine (http://www.matrixscience.com/ search_form_select.html). The criteria for positive identification of proteins were set as follows: filter by protein score > 10, filter peptide by score > 8, and percentage scored peak intensity (% SPI) > 70 (67).

2.15. Western blotting

Ten micrograms of WT and *Fabp7* KO (astrocyte lysate) were separated on a SDS-PAGE gel (15%), transferred onto a polyvinylidene difluoride membrane (Immobilon-P; Millipore, Bedford, MA, USA), and blocked with tris-buffered saline (TBS) containing 0.1% Tween 20 (Sigma-Aldrich) and 5% skimmed milk for 1 h at room temperature. Membranes were incubated with specific primary antibodies, including rabbit anti-FABP7 (0.125 μg/ml) (31), rabbit anti-PEA-15 (1:500; Santa Cruz Biotech, Santa Cruz, CA, USA), mouse anti-vimentin (1:500; Abcam, Cambridge, UK), rat anti-GFAP (1:2500; Invitrogen) and mouse anti-β-actin (1:5000; Santa Cruz Biotech) overnight at 4 °C. Subsequently, membranes were incubated with HRP-conjugated secondary antibodies, including goat anti-rabbit (1:2000; Chemicon, Temecula, CA), goat anti-rat (1:1000; Chemicon), and goat anti-mouse (1:5000; Chemicon) for 1 h at room temperature, and developed with an ECL Western blot detection kit (Amersham Pharmacia Biotech, Piscataway, NJ, USA). The images of blots were captured using Image Reader LAS-1000 (Fujifilm, Tokyo, Japan) and the intensity of protein bands were analyzed using Multi Gauge software (Fujifilm). Totally two sets of Western blot (at least three biological replicates per each experiment) were performed and expression levels of proteins of interest (PEA-15 and vimentin) were normalized to the expression of β-actin, as a control for loading.

2.16. Statistics

All results are presented as mean ± SEM of at least three independent experiments or at least four individual animals (in the case of *in vivo* experiments) with at least three biological replicates. Statistical analyses were conducted with SPSS software (version 13.0; SPSS Inc, Chicago, IL). I used *t*-test except for electrophysiological data and Western blotting, which were analyzed using Mann-Whitney U test. $P < 0.05$ was considered statistically significant.

3. RESULTS

3.1. Dendritic complexity and spine density is altered in the prefrontal cortex of FABP7-deficient mice

I first examined the localization pattern of FABP7 in the mouse mPFC. Consistent with our former findings in the mouse cerebral cortex (31, 33, 34), FABP7 was localized in the mPFC in $GFAP^+$ astrocytes [**Fig. 3.1A**] and $PDGFR\alpha^+$ oligodendrocyte progenitor cells [**Fig. 3.1B**] but not in $MAP2^+$ neurons [**Fig. 3.1C**] or $CD11b^+$ microglia [**Fig. 3.1D**].

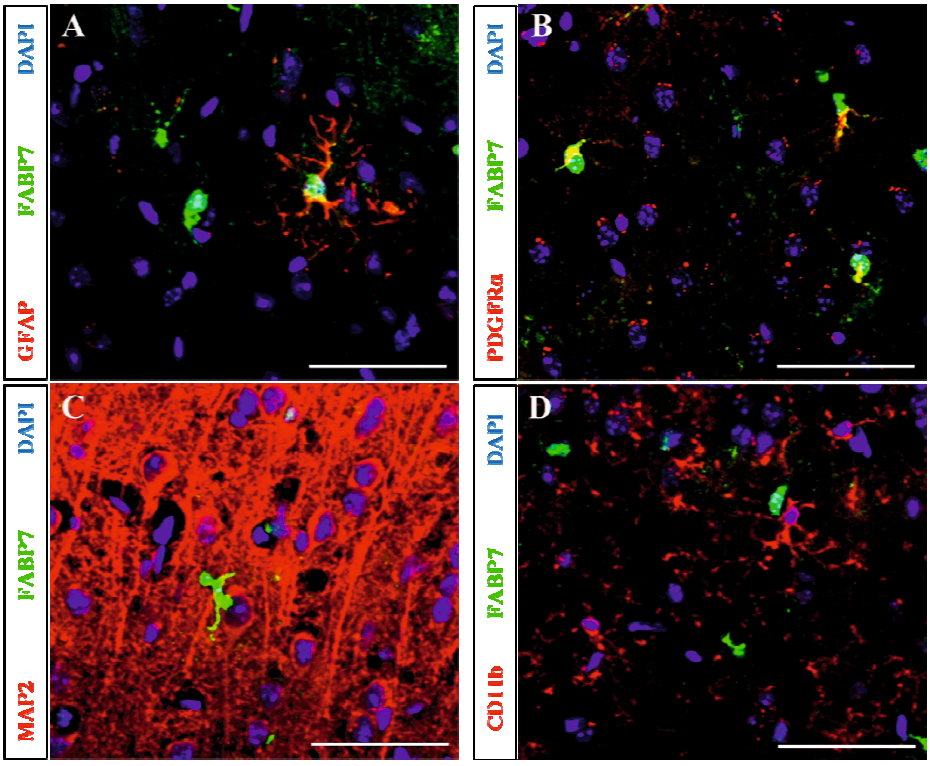

Fig. 3.1 Identification of FABP7-expressing cells in the mPFC of normal mouse brain. Immunofluorescence micrographs indicate expression of FABP7 in the mPFC of mouse brain. Expression of FABP7 in astrocytes (**A**) and oligodendrocyte progenitor cells (OPCs) (**B**) was confirmed by co-localization of FABP7 (green) with GFAP (red) and PDGFRα (red), respectively.

No FABP7 expression was found in MAP2$^+$ neurons (**C**) and CD11b$^+$ microglia cells (**D**). Scale bars: 50 μm.

Furthermore, the mPFC of *Fabp7* KO mice showed no significant difference from WT mice in the population density of NeuN$^+$ neurons [151 ± 3.3 cells/0.08 mm^2 in WT vs. 146 ± 2.3 cells/0.08 mm^2 in *Fabp7* KO, $P = 0.27$; Fig. **Fig. 3.2A-C**], GFAP$^+$ astrocytes [6.6 ± 0.5 cells/0.08 mm^2 in WT vs. 6.4 ± 0.5 cells/0.08 mm^2 in *Fabp7* KO, $P = 0.69$; **Fig. 3.2D-F**] and OLIG2$^+$ oligodendrocyte lineage cells [7.2 ± 0.3 cells/0.08 mm^2 in WT vs. 6.8 ± 0.3 cells/0.08 mm^2 in *Fabp7* KO, $P = 0.28$; **Fig. 3.2G-I**].

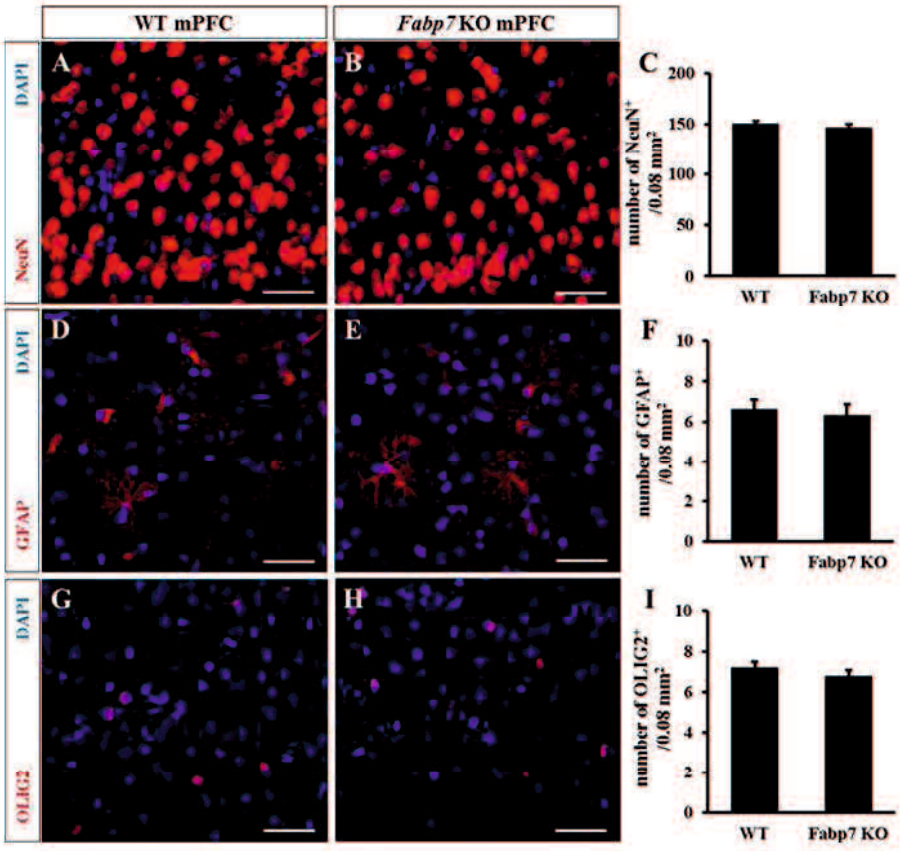

Fig. 3.2 The population density of neural cells in the mPFC of *Fabp7* KO mice. Immunofluorescence micrographs showing cells labeled with specific markers for neurons (NeuN, A, B), astrocytes (GFAP, D, E) and oligodendrocyte lineage cells (OLIG2, G, H) in the mPFC of

Fabp7 KO mice and their WT littermates. Bar graphs represent the population density of neurons (C), astrocytes (F), and oligodendrocyte progenitor cells (OPCs) (I) in the mPFC of *Fabp7* KO mice compared with those in their WT littermates. Data are presented as mean ± SEM of images (0.08 mm2) from *Fabp7* KO (n > 90 images) and WT (n > 90 images) mPFC (n = 4 mice/genotype). **P* < 0.05; scale bars: 50 μm.

Next, to explore the possibility that a FABP7 deficiency may lead to alterations in neuronal morphology *in vivo*, including spine density, I performed Golgi staining on the age- and background-matched *Fabp7* KO and WT mice, and analyzed the morphological characteristics of pyramidal neurons in the mPFC. Notably, a Sholl analysis examining dendritic complexity revealed that the pyramidal neurons of *Fabp7* KO mice showed less complex dendritic trees than their WT counterparts for both basal and apical dendrites [**Fig. 3.3A-D**]. The morphometric analyses of pyramidal neuron dendrites revealed that the number of dendritic branches [32.5 ± 1.46 in WT vs. 19.8 ± 0.75 in *Fabp7* KO, $P < 0.001$], the total length of dendritic branches [3480 ± 140 μm in WT vs. 2209 ± 78 μm in *Fabp7* KO, $P < 0.001$], and the extent of the area covered by the dendritic arbor [74654 ± 3067 μm^2 in WT vs. 59738 ± 3422 μm^2 in *Fabp7* KO, $P < 0.001$] were significantly decreased in *Fabp7* KO mice compared with those in WT mice [**Fig. 3.3E-G**].

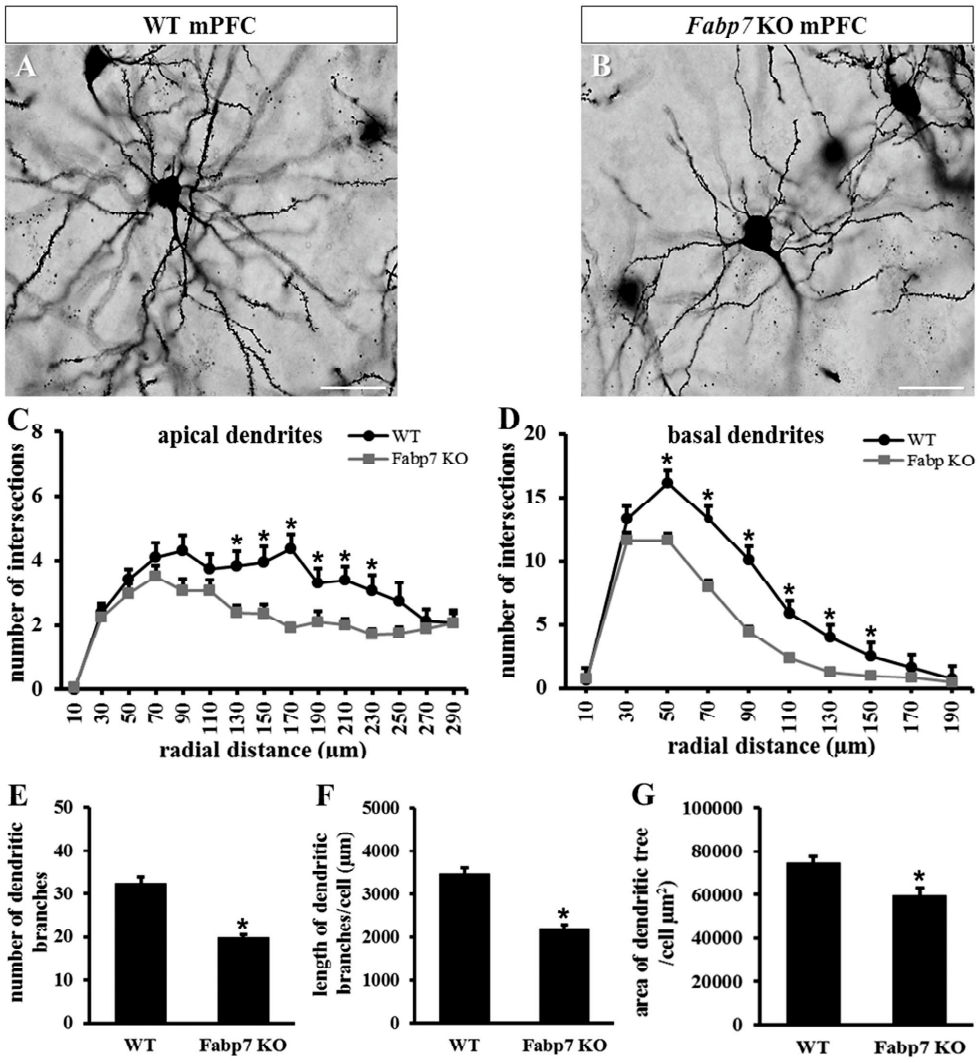

Fig. 3.3 Alteration of neuronal dendritic morphology in the mPFC of *Fabp7* KO mice. Phase contrast micrographs show representative Golgi stained layer II/III pyramidal neurons in the mPFC of wild-type (WT) (A) and *Fabp7* KO (B) mice. Line charts represent Sholl analysis results for apical (C) and basal (D) dendrites of *Fabp7* KO and WT mice. Bar graphs represent analyses of the number of dendritic branches per cell (E), total length of dendritic branches per cell (F) and area covered by the dendritic tree (G) of pyramidal neurons in the mPFC of *Fabp7* KO and WT mice. Data are presented as mean ± SEM from pyramidal neurons of *Fabp7* KO (n = 41 neurons) and WT (n = 39 neurons) mice (n = 5 mice/genotype); **P* < 0.05; scale bars: 50 μm.

I also found that the dendritic spine density of cortical pyramidal neurons for apical [0.96 ± 0.02/μm of dendrite in WT vs. 0.83 ± 0.02/μm of dendrite in *Fabp7* KO, $P < 0.001$] and basal dendrites [1.0 ± 0.02/μm of dendrite in WT vs. 0.84 ± 0.03/μm of dendrite in *Fabp7* KO, $P < 0.001$] was significantly decreased in *Fabp7* KO mice compared with that in WT mice [**Fig. 3.4A-C**].

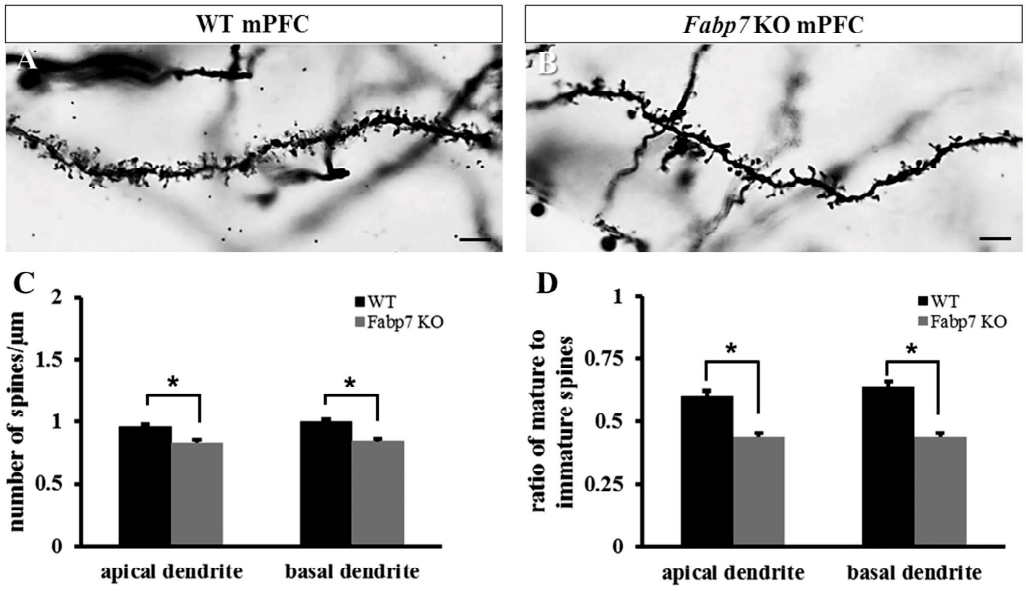

Fig. 3.4 Alteration of density and maturity of dendritic spines in the mPFC of FABP7-deficient mice. High-magnification phase contrast micrographs show dendritic spines of pyramidal neurons in the mPFC of WT (**A**) and *Fabp7* KO (**B**) mice. Bar graphs represent the spine density (**C**) and ratio of mature to immature spines (**D**) in the apical and basal dendrites of pyramidal neurons. Data are presented as mean ± SEM from dendrites of *Fabp7* KO (n = 39 apical dendrites and n = 40 basal dendrites) and WT (n = 43 apical dendrites and n = 39 basal dendrites) pyramidal neurons (n = 5 mice/genotype); $*P < 0.05$; scale bars: 5 μm.

Moreover, the ratio of stubby, mushroom-shaped mature spines to thin, filopodium-like immature spines was significantly decreased in *Fabp7* KO mice compared with that in WT mice [0.6 ± 0.02 in WT vs. 0.44 ± 0.01 in *Fabp7* KO for apical dendrites, $P < 0.001$; 0.64 ± 0.02 in

WT vs. 0.44 ± 0.01 in *Fabp7* KO for basal dendrites, $P < 0.001$; **Fig. 3.4D**]. Thus, these results indicate that a FABP7 deficiency in cortical astrocytes is associated with a reduction in dendritic complexity, spine density and maturity of spines in cortical pyramidal neurons *in vivo*.

3.2. Neuronal morphology is altered in FABP7-deficient neuron-enriched mixed cortical cultures

To further explore the possibility that astrocytic FABP7 is involved in the regulation of neuronal dendritic formation, neuron-enriched primary mixed cortical cultures were established from *Fabp7* KO and WT mice (P0-P1). Under the appropriate culture conditions, neurons can mimic many essential properties of neurons *in vivo*, develop asymmetrical distributions of axonal and dendritic proteins, produce dendritic arborization, and form synapses (68).

Using a cell survival assay, we first confirmed that the FABP7 deficiency in astrocytes had no obvious impact on the viability of cortical neurons [**Fig. 3.5A**]. After 7 days, the survival of neurons in *Fabp7* KO cultures showed no significant difference from that in WT cultures [67.2 ± 2.34 % in WT vs. 57.31 ± 10.2 % in *Fabp7* KO, $P = 0.67$; **Fig. 3.5B**].

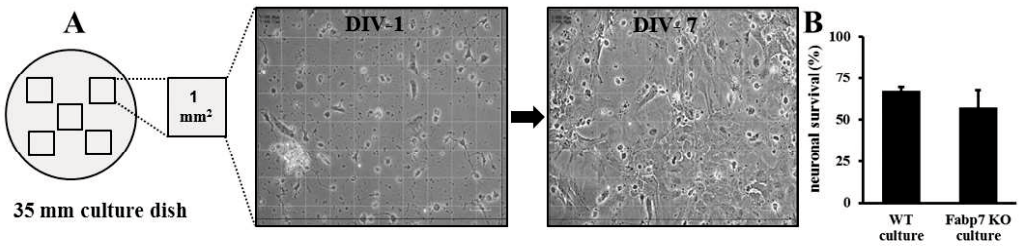

Fig. 3.5 Viability of neurons in culture is not influenced by FABP7 deficiency. Scheme shows the cell survival assay that was used to evaluate viability of neurons in neuron-enriched mixed cortical cultures (**A**, for a detailed explanation, see Methods part). Bar graph represents the percentage of surviving neurons in WT and *Fabp7* KO mixed cortical cultures at DIV-7 (**B**). Data

are presented as mean ± SEM of five images per culture dish from three independent experiments (three dishes/genotype/independent experiment).

I next examined the dendritic morphology of pyramidal neurons in the two genotypes at DIV-7 and found that compared with those in WT cultures, neurons in *Fabp7* KO cultures [**Fig. 3.6B**] exhibited aberrant dendritic morphology [**Fig. 3.6A**] and showed a significant decrease in the total length of dendritic branches [563 ± 20.2 μm in WT vs. 497 ± 20.1 μm in *Fabp7* KO, $P = 0.02$; **Fig. 3.6D**] and the extent of the area covered by the dendritic tree [10932 ± 535 in WT vs. 9241 ± 535 μm^2 in *Fabp7* KO, $P = 0.03$; **Fig. 3.6E**]. The number of neuronal dendritic branches in *Fabp7* KO cultures was lower than that in WT cultures, although this was not statistically significant [22.8 ± 1.2/neuron in WT vs. 20.7 ± 1.1/neuron in *Fabp7* KO, $P = 0.19$; **Fig. 3.6C**]. These results indicate that a FABP7 deficiency in astrocytes may cause abnormal neuronal dendritic morphology in neuron-enriched mixed cortical cultures.

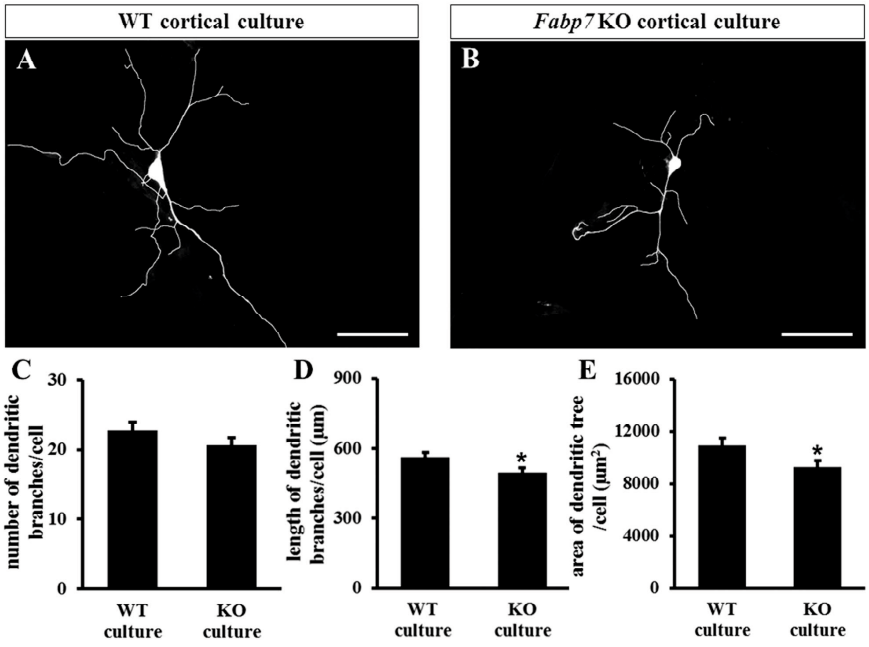

Fig. 3.6 Alteration of neuronal morphology in FABP7-deficient neuron-enriched primary mixed cortical cultures. Immunofluorescence micrographs show representative neurons at DIV-

7 stained with the MAP2 antibody in neuron-enriched mixed cortical cultures prepared from WT (**A**) and *Fabp7* KO (**B**) mice. Bar graphs represent the number of dendritic branches per cell (**C**), total length of dendritic branches per cell (**D**) and area covered by the dendritic tree (**E**) of cortical neurons in WT and *Fabp7* KO neuron-enriched mixed cortical cultures. Data are presented as mean ± SEM from neurons of *Fabp7* KO (n = 184 neurons) and WT (n = 219 neurons) cultures; **P* < 0.05; scale bars: 50 μm.

3.3. Neuronal morphology is altered in FABP7-deficient neuron-astrocyte co-cultures

To more clearly elucidate the role of FABP7 expressed by astrocytes on neuronal dendritic formation, a tractable dissociated neuron-astrocyte co-culture was established. Cortical embryonic neurons were dissociated from timed pregnant WT dams (E17) and then co-cultured with either WT or *Fabp7* KO astrocytes. After 7 days of co-culture, the morphological characteristics of the neurons co-cultured with either WT or *Fabp7* KO astrocytes were evaluated.

As expected, WT neurons co-cultured with *Fabp7* KO astrocytes exhibited altered dendritic morphology [**Fig. 3.7B**] compared with those co-cultured with WT astrocytes [**Fig. 3.7A**]. The density of dendritic branches [29.2 ± 0.6 in WT co-culture vs. 22.9 ± 0.5 in *Fabp7* KO co-culture, $P < 0.001$; **Fig. 3.7C**], total length of dendritic branches [1487 ± 28.4 μm in WT co-culture vs. 1189 ± 23.4 μm in *Fabp7* KO co-culture, $P < 0.001$; **Fig. 3.7D**] and extent of the area covered by dendritic tree [40886 ± 942 μm^2 in WT co-culture vs. 34275 ± 870 μm^2 in *Fabp7* KO co-culture, $P < 0.001$; **Fig. 3.7E**] of WT cortical neurons were significantly reduced for those neurons grown with FABP7-deficient astrocytes.

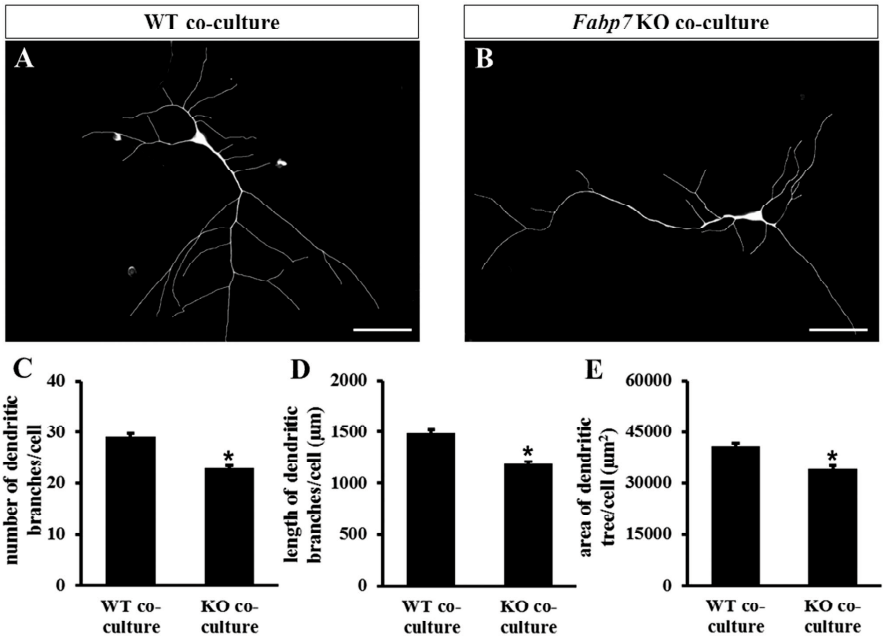

Fig. 3.7 Alteration of neuronal morphology in FABP7-deficient neuron-astrocyte co-culture. Immunofluorescence micrographs show representative WT cortical neurons co-cultured with WT (**A**) or *Fabp7* KO (**B**) astrocytes after 7 days in co-culture stained with the MAP2 antibody. Bar graphs represent the number of dendritic branches per cell (**C**), total length of dendritic branches per cell (**D**) and area covered by the dendritic tree (**E**) of cortical neurons co-cultured with WT or *Fabp7* KO astrocytes. Data are presented as mean ± SEM from cortical neurons co-cultured with *Fabp7* KO (n = 277 neurons) and WT (n = 295 neurons) astrocytes; **P* < 0.05; scale bars: 50 μm.

By contrast, there was no significant difference in the population density *Fabp7* KO and WT astrocytes in co-cultures [9.8 ± 0.5/0.05 mm^2 and 10.6 ± 0.6/0.05 mm^2, respectively, P = 0.32; Fig. **Fig. 3.8A-C**], suggesting that these results are not attributable to deviations in the population density of astrocytes in co-cultures.

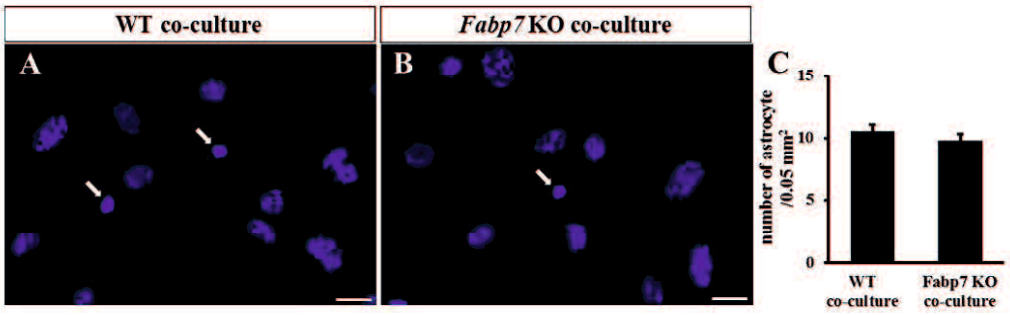

Fig. 3.8 No significant difference is detected in the population density of astrocytes between WT and FABP7-deficient co-cultures. Fluorescence micrographs show WT (**A**) and *Fabp7* KO (**B**) co-cultures stained with DAPI nuclei stain (blue) after 7 days of incubation. Astrocytes were detected by their large and bean-shaped nuclei containing several nucleoli, and neurons were identified by their smaller and compact round-shaped nuclei (white arrows). Bar graph represents the number of astrocytic nuclei in random microscopic images (0.05 mm^2) captured from *Fabp7* KO and WT co-cultures (**C**). Data are presented as mean ± SEM of 20 images/coverslip from three independent experiments of co-cultures with *Fabp7* KO and WT astrocytes (three coverslips/astrocyte genotype/independent experiment); scale bars: 20 μm.

Taken together, these data confirm that FABP7-deficient astrocytes cannot fully support normal dendritic arborization of cortical neurons, indicating that astrocytic FABP7 may be an important factor regulating the formation of accurate cortical neuronal networks.

3.4. Neuronal morphology is altered in cortical neurons cultured with ACM derived from FABP7-deficient astrocytes

The regulatory roles of astrocyte-expressed FABP7 on neuronal morphology may be mediated through humoral factors. To evaluate this hypothesis, I established a cortical neuronal culture system using ACM. WT embryonic neurons (E17) were cultured on coated glass coverslips, and the medium was replaced with ACM obtained either from *Fabp7* KO or WT astrocyte cultures;

the population density of the astrocytes was standardized, with no significant difference detected between the two genotypes (data not shown).

I found no significant difference in the population density of cortical neurons treated with either *Fabp7* KO or WT ACM for 7 days [4.1 ± 0.6 and 4.6 ± 0.4, respectively, $P = 0.52$; **Fig. 3.9A-C**], suggesting that *Fabp7* KO ACM had no obvious impact on neuronal survival.

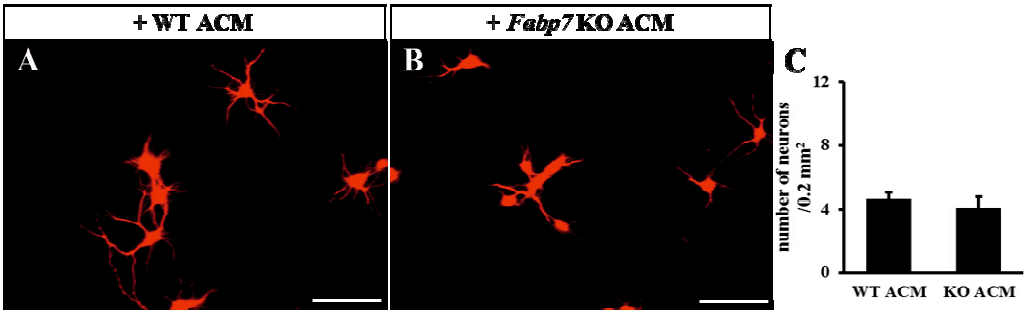

Fig. 3.9 No significant difference is detected in population densities from cortical neurons cultured with ACM derived from WT or FABP7-deficient astrocytes. Immunofluorescence micrographs showing WT cortical neurons stained with MAP2 antibody (red) after 7 days of incubation with ACM prepared from WT (**A**) or *Fabp7* KO (**B**) astrocytes. Bar graph represents the number of $MAP2^+$ neurons in random microscopic images (0.2 mm^2) captured from neuronal cultures with *Fabp7* KO or WT ACM (**C**). Data are presented as mean ± SEM of five images/coverslips from three independent experiments (three coverslips/ACM genotype/independent experiment); scale bars: 100 μm.

However, cortical neurons cultured in *Fabp7* KO ACM showed significant differences in their dendritic morphology compared with those cultured in WT ACM [**Fig. 3.10A,B**] for the total number of dendritic branches [18.2 ± 0.4 in WT ACM vs. 15.2 ± 0.4 in *Fabp7* KO ACM, $P < 0.001$; **Fig. 3.10C**], total length of dendritic branches [647 ± 14.2 μm in WT ACM vs. 462 ± 12.5 μm in *Fabp7* KO ACM, $P < 0.001$; **Fig. 3.10D**], and extent of the area covered by dendritic

trees [1410 ± 39.4 μm^2 in WT ACM vs. 1102 ± 39.9 μm^2 in *Fabp7* KO ACM, $P < 0.001$; **Fig. 3.10E**]. Therefore, it is likely that astrocytic FABP7 humorally regulates neuronal morphology.

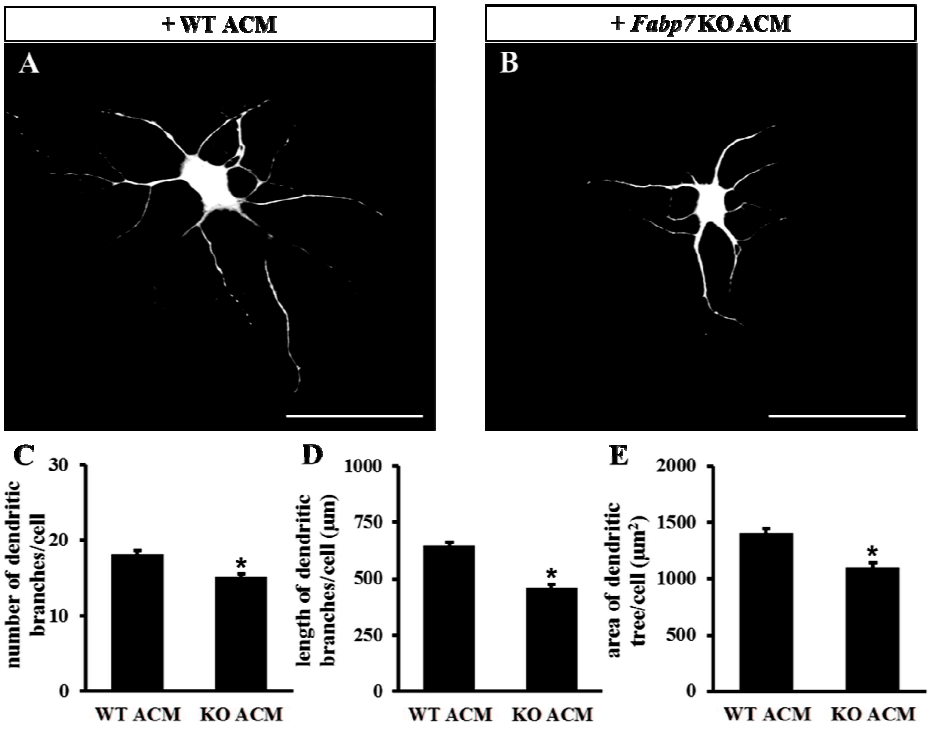

Fig. 3.10 Alteration of neuronal morphology in cortical neurons cultured with ACM prepared from FABP7-deficient astrocytes. Immunofluorescence micrographs show representative WT cortical neurons treated with ACM prepared from WT (**A**) or *Fabp7* KO (**B**) astrocytes for 7 days and stained with MAP2 antibody. Bar graphs represent the number of dendritic branches per cell (**C**), total length of dendritic branches per cell (**D**) and area covered by the dendritic tree (**E**) of cortical neurons cultured with ACM from WT or *Fabp7* KO astrocytes. Data are presented as mean ± SEM from cortical neurons treated with ACM from *Fabp7* KO (n = 304 neurons) and WT (n = 301 neurons) astrocytes; *$P < 0.05$; scale bars: 50 μm.

3.5. FABP7 deficiency in astrocytes impairs synapse formation

Dendritic spines provide the sites for most of the excitatory synaptic inputs on pyramidal neurons (69). Therefore, I next examined the impact of a FABP7 deficiency on excitatory synapse

formation. The density of excitatory synapses in the mPFC as indicated by the co-localization of VGlut1$^+$ and PSD95$^+$ puncta showed a 30% decrease in *Fabp7* KO mice compared with that in WT mice [28.2 ± 2.3 in WT and 19.6 ± 1.4 in *Fabp7* KO, $P = 0.002$; **Fig. 3.11 A-C**].

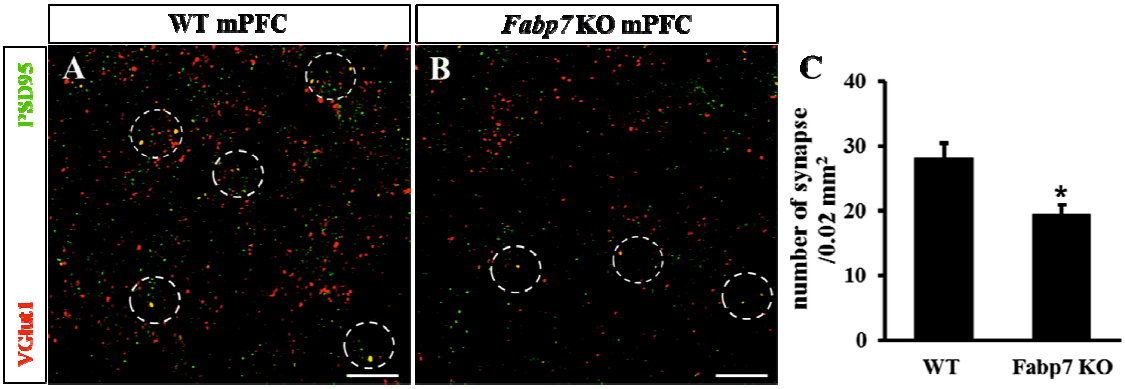

Fig. 3.11 Alteration of excitatory synapse formation in the mPFC of *Fabp7* KO mice. High-magnification immunofluorescence micrographs show synaptic staining in the mPFC of WT (**A**) and *Fabp7* KO (**B**) mice. Synapses (yellow puncta) are detected by co-localization of the presynaptic marker VGlut1 (red) and postsynaptic marker PSD95 (green). White dashed circles highlight some of the synapses. Bar graph represents the number of synapses in the mPFC (layer II/III, 0.02 mm^2) of *Fabp7* KO and WT mice (C). Data are presented as mean ± SEM from images of *Fabp7* KO (n = 51 images) and WT (n = 51 images) mPFC (n = 4 mice/genotype). *$P < 0.05$; scale bars: 20 μm.

Consistent with this finding, cortical neurons grown over a monolayer of WT astrocytes developed more excitatory synapses, as indicated by the co-localization of synaptophysin$^+$ and PSD95$^+$ puncta, than neurons grown with *Fabp7* KO astrocytes [1.78 ± 0.2 and 1.27 ± 0.1, respectively, $P = 0.014$; **Fig. 3.12A-C**].

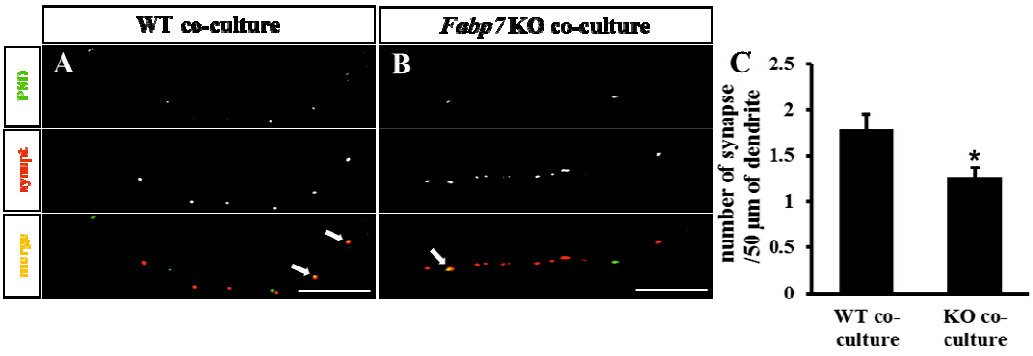

Fig. 3.12 Alteration of excitatory synapse formation in the cortical neurons co-cultured with FABP7-deficient astrocytes. High-magnification immunofluorescence micrographs show dendritic segments of WT cortical neurons after 7 days co-culture with WT (A) or *Fabp7* KO (B) astrocytes stained with synaptic markers. Synapses are detected by co-localization (yellow puncta, white arrows in lower panels) of the presynaptic marker synaptophysin (middle panels) and postsynaptic marker PSD95 (upper panels). Bar graph represents the density of excitatory synapses per 50 μm of dendrites (C). Data are presented as mean ± SEM from neurons co-cultured with *Fabp7* KO (n = 60 neurons, three segments/neuron) and WT (n = 60 neurons, three segments/neuron) astrocytes; **P* < 0.05; scale bars: 10 μm.

3.6. Excitatory synaptic transmission is decreased in the mPFC of FABP7-deficient mice

To further examine whether alterations in the dendritic spine density and reduction in the excitatory synapse formation in the mPFC of *Fabp7* KO mice were also reflected at electrophysiological level, whole-cell patch-clamp recordings in the acute brain slices were performed [**Fig. 3.13**]. The mEPSCs were recorded to investigate whether deficiency of FABP7 affects the excitatory synaptic transmission into mPFC pyramidal neurons [**Fig. 3.13A**]. In accordance with the morphological results, cortical pyramidal neurons in the mPFC of *Fabp7* KO mice exhibited significant reduction in frequency [36.39 ± 8.40 events/5 min in WT vs. 19.95 ± 3.97 events/5 min in *Fabp7* KO, *P* = 0.01; **Fig. 3.13B**] and amplitude [17.08 ± 0.46 pA

in WT vs. 13.94 ± 0.39 pA in *Fabp7* KO, $P < 0.001$; **Fig. 3.13C**] of mEPSCs in comparison with WT counterparts.

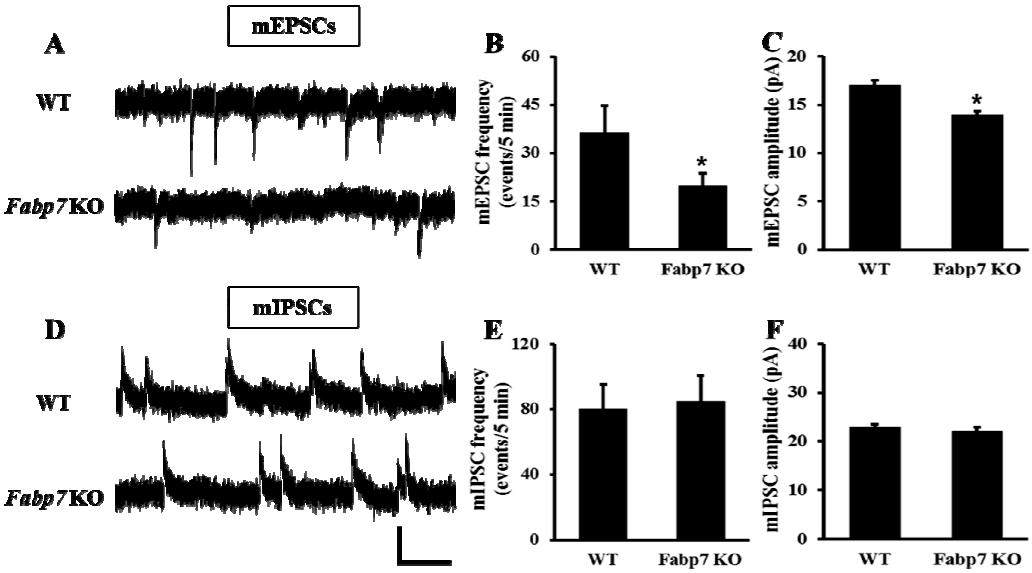

Fig. 3.13 Excitatory synaptic transmission is decreased in pyramidal neurons in the mPFC of FABP7-deficient mice. Representative traces from whole-cell patch-clamp recordings of mEPSCs from pyramidal neurons in layer II/III mPFC of *Fabp7* KO and WT mice (**A**). The mEPSCs were recorded at holding potential of -60 mV for 5 min in the presence of TTX (0.5μM). Bar graphs represent analyses of the frequency (**B**) and amplitude (**C**) of recorded mEPSCs from *Fabp7* KO (n = 55 cells) and WT (n = 56 cells) mice. Representative traces of mIPSCs from layer II/III pyramidal neurons in the mPFC of *Fabp7* KO and WT mice (**D**). The mIPSCs were recorded at holding potential of 0 mV for 5 min in the presence of TTX (0.5μM). Bar graphs represent analyses of the frequency (**E**) and amplitude (**F**) of recorded mIPSCs from *Fabp7* KO (n = 35 cells) and WT (n = 34 cells) mice. Data are presented as mean ± SEM of neurons recorded from four mice per genotype; Mann-Whitney U test, $*P < 0.05$; vertical scale bar: 20 pA; horizontal scale bars: 200 ms.

I next examined whether inhibitory synaptic transmission was also affected in the mPFC of *Fabp7* KO mice, by whole-cell recordings of mIPSCs [**Fig. 3.13D**]. Pyramidal neurons in the

mPFC of *Fabp7* KO mice showed no significant difference in mIPSCs frequency [80.74 ± 14.61 events/5 min in WT vs. 85.14 ± 15.47 events/5 min in *Fabp7* KO, $P = 0.74$; **Fig. 3.13E**] and amplitude [22.94 ± 0.60 pA in WT vs. 22.10 ± 0.73pA in *Fabp7* KO, $P = 0.35$; **Fig. 3.13F**] in comparison with WT counterparts. These results suggest that FABP7-deficiency in astrocytes has selectively impacted on excitatory, but not inhibitory, basal synaptic functions in the mPFC of *Fabp7* KO mice.

3.7. Transplantation of WT astrocytes rescues altered behavioral phenotypes in FABP7-deficient mice

We recently reported on hyperactivity and anxiety-related phenotypes in *Fabp7* KO mice and suggested the possible involvement of *FABP7* mutations in the pathology of human neuropsychiatric illnesses, including schizophrenia (42) . Here, I found that the total distance traveled [1526 ± 113 cm in WT vs. 2720 ± 107 cm in *Fabp7* KO, $P < 0.001$; **Fig. 3.14A**], total time spent traveling [84.8 ± 4.6 s in WT vs. 117 ± 3.6 s in *Fabp7* KO, $P < 0.001$; **Fig. 3.14B**] and number of crossings between squares [235 ± 22.3 in WT vs. 289 ± 14.2 in *Fabp7* KO, $P = 0.04$; **Fig. 3.14C**] were significantly increased in *Fabp7* KO mice compared with those values in their WT littermates, consistent with our recent findings (42). To determine whether the transplantation of WT astrocytes into the mPFC could rescue the hyperactive phenotype of the *Fabp7* KO mice, GFP-expressing WT and *Fabp7* KO astrocytes were locally transplanted into the mPFC of *Fabp7* KO mice at P56. The effect of the transplants was evaluated using the open field test on P70 (14 days after the transplantation). Notably, the transplantation of WT astrocytes significantly rescued most of the hyperactive phenotype in *Fabp7* KO mice, as compared with vehicle-injected control mice, including the total time spent traveling [125 ± 5.5 s in WT astrocyte transplanted vs. 141 ± 4.5 s in control, $P = 0.04$; **Fig. 3.14E**] and number of

crossings between squares [350 ± 20.6 in WT astrocyte transplanted vs. 405 ± 16.9 in control, *P* = 0.04; **Fig. 3.14F**]. By contrast, no significant improvement was noted in the hyperactive phenotype of *Fabp7* KO mice in the open field test after transplantation of *Fabp7* KO astrocytes [**Fig. 3.14D-F**]. These results suggest that a FABP7 deficiency in mPFC astrocytes is associated with the hyperactive phenotype in *Fabp7* KO mice.

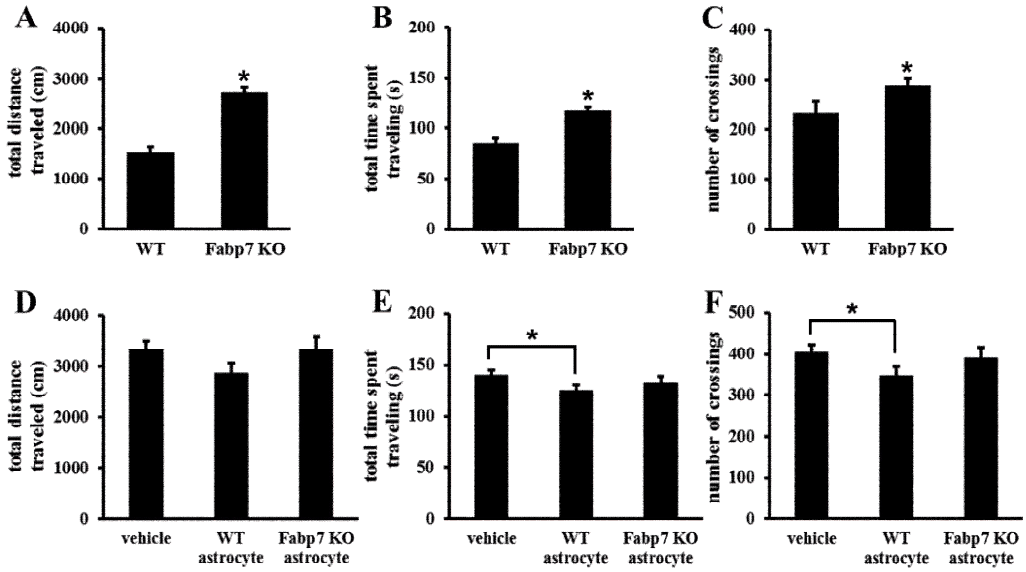

Fig. 3.14 Astrocyte transplantation partially rescues behavioral phenotype in *Fabp7* KO mice. Bar graphs represent the results of the behavioral analysis for *Fabp7* KO and WT mice in the open field test. *Fabp7* KO mice show increased distance traveled (**A**), time spent traveling (**B**) and number of crossings between intersections of the field (**C**) compared with their WT littermates. Data are presented as mean ± SEM in *Fabp7* KO (n = 18) and WT (n = 16) mice; **P* < 0.05. Bar graphs showing the results of behavioral analysis of *Fabp7* KO mice in the open field test 14 days after transplantation (astrocytes or vehicle microinjection). Transplantation of WT but not *Fabp7* KO astrocytes into the mPFC of *Fabp7* KO mice improve performance of mice in the open field test by decreasing traveling time (**E**) and the number of crossings (**F**) compared with those measures in the control group. Transplantation of astrocytes into the mPFC of *Fabp7* KO mice has no significant impact on the distance traveled in the open field test (**D**). Data are

presented as mean ± SEM from *Fabp7* KO mice receiving WT astrocytes (n = 14 mice), *Fabp7* KO astrocytes (n = 15 mice) or a PBS microinjection (n = 14 mice); **P* < 0.05.

3.8. Detection of spots with differential expression between WT and *Fabp7* KO astrocytes on 2-DE gels

Protein expressions by primary cultured astrocytes from WT and *Fabp7* KO mice were assessed by 2-DE (five biological and two technical replicates for each genotype). Protein spots were visualized with a fluorescent gel staining and differences in the spot intensities between the two genotypes were analyzed and quantified by Progenesis Samespots software. At least 16 protein spots showed altered expression in *Fabp7* KO astrocytes [**Fig. 3.15**]. By visual assessment one spot was almost absent in *Fabp7* KO gels (spot number 16) which was expected to be FABP7 [**Fig. 3.15A**]. Seven spots showed increased intensities and nine spots showed decreased intensities in *Fabp7* KO astrocytes [**Fig. 3.15A,B**].

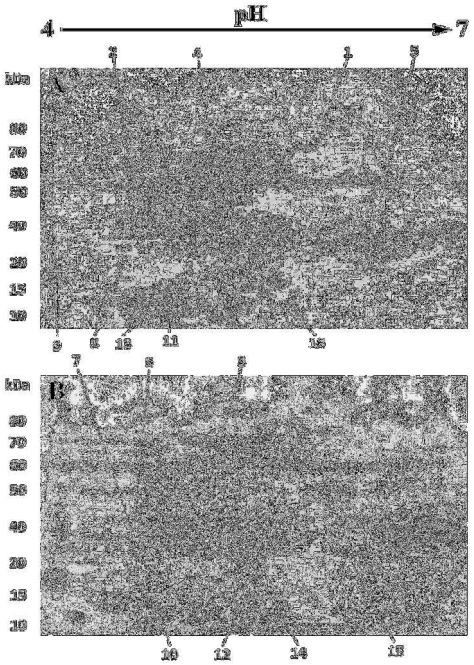

Fig. 3.15 Representative images of 2-DE gels of WT and *Fabp7* KO astrocytes stained with fluorescent dye (Flamingo Gel Stain). Protein spots whose expression levels were different

between *Fabp7* KO and WT astrocytes are numbered and pointed out by arrows. Nine protein spots show reduction and seven other protein spots represent higher expression in *Fabp7* KO astrocytes (**B**) in comparison with WT counterparts (**A**). Spot number 16 expected to be FABP7 due to its absence in the *Fabp7* KO gel.

3.9. Identification of proteins

The spots with differential expressions between the two genotypes were digested and forwarded for identification by LC-MS/MS. The result of protein identification is summarized in **Table 3.1**. Among 16 differentially expressed spots, four spots with more than two distinct peptides (≥ 2) or MS/MS search scores over 30 were selected for further confirmation by Western blotting. These proteins included FABP7, GFAP, PEA-15, and vimentin.

Table 3.1. Identification of proteins that are differentially expressed between *Fabp7* KO and WT astrocytes by LC-MS/MS analysis.

spot	protein name	abbreviated gene name	accession no.	theoretical *pI*	theoretical *M*r	distinct peptides	sequence coverage (%)	MS/MS search score	change in *Fabp7* KO astrocyte (fold)	*P*
1	mitochondrial 10-formyltetrahydrofolate dehydrogenase	*Aldh1l2*	Q8K009	5.5 - 6	70 - 80	1	1	10.65	- 2	0.009
2	vimentin	*Vim*	P20152	4.5 - 5	40 - 50	3	10	34.33	- 1.6	0.015
3	glial fibrillary acidic protein	*Gfap*	P03995	5	40 - 50	2	10	28.81	+ 1.6	0.013
4	actin, aortic smooth muscle	*Acta2*	P62737	5 - 5.5	40 - 50	1	2	17.37	- 1.3	0.049
5	nuclear receptor corepressor 1	*Ncor1*	Q60974	6 - 6.5	50 - 60	1	0	11.36	- 1.4	0.039
6	COP9 signalosome complex subunit 4	*Cops4*	O88544	4.5 - 5	40 - 50	1	4	11.15	+ 1.2	0.023
7	melanoma inhibitory activity protein 3	*Mia3*	Q8BI84	4.5 - 5	30 - 40	1	0	10.72	+ 1.4	0.017
8	protein BUD31 homolog	*Bud31*	Q6PGH1	4 - 4.5	15 - 20	1	20	10.14	- 1.5	0.038
9	calmodulin	*Calm1*	P62204	4.5	15 - 20	1	10	16.58	- 1.4	0.036
10	DnaJ homolog subfamily C member 5	*Dnajc5*	P60904	4.5	10 - 15	1	10	10.33	+ 1.1	0.031
11	hippocalcin-like protein 1	*Hpcal1*	P62748	4.5 - 5	15 - 20	1	10	11.17	- 1.2	0.048
12	serrate RNA effector molecule homolog	*Srrt*	Q99MR6	5	10 -15	1	2	10.76	+ 1.3	0.031
13	astrocytic phosphoprotein PEA-15	*Pea15*	Q62048	5	10 -15	3	12	40.67	- 1.3	0.016
14	ganglioside GM2 activator	*Gm2a*	Q60648	5	20 - 30	1	5	11.63	+ 1.3	0.027
15	ataxin-7-like protein 3	*Atxn7l3*	A2AWT3	5.5 - 6	20 -30	1	5	10.63	+ 1.6	0.044
16	fatty acid binding protein, brain	*Fabp7*	P51880	5.5 - 6	10 - 15	3	31	38.79	- 2.1	0.003

3.10. Decreased expression of vimentin and PEA-15 in *Fabp7* KO astrocytes

Western blotting analysis was performed and confirmed the significant decrease in the expression of vimentin [1.57 ± 0.07 in WT astrocytes vs. 0.52 ± 0.19 in *Fabp7* KO astrocytes, $P = 0.03$; **Fig. 3.16A,B**] and PEA-15 [1.51 ± 0.18 in WT astrocytes vs. 0.8 ± 0.09 in *Fabp7* KO astrocytes, $P = 0.03$; **Fig. 3.16A,B**] proteins in *Fabp7* KO astrocytes compared to WT astrocytes. Moreover, expression of FABP7 was not discerned in *Fabp7* KO astrocyte samples which further confirm the authenticity of our experiments [**Fig. 3.16A**]. However, Western blotting results did not confirm GFAP upregulation in *Fabp7 KO* astrocytes and no change was detected in the expression of GFAP between *Fabp7* KO and WT astrocytes [2.03 ± 0.52 in WT astrocytes vs. 2.11 ± 0.39 in *Fabp7* KO astrocytes, $P = 0.89$ **Fig. 3.16A,B**].

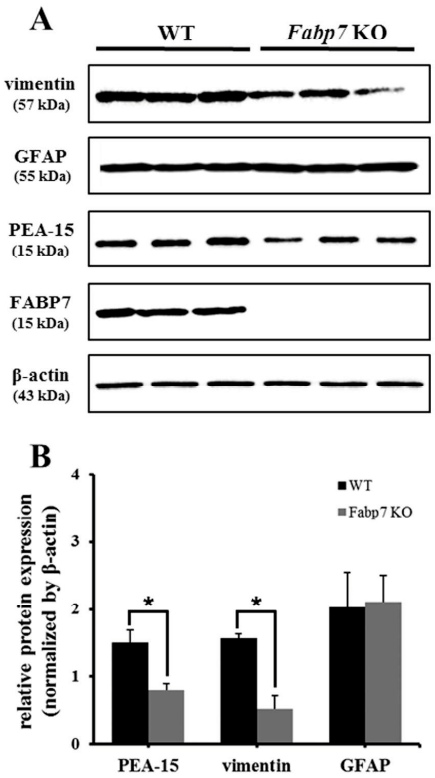

Fig. 3.16 Protein levels of FABP7, GFAP, PEA-15 and vimentin in WT and *Fabp7* KO astrocytes were evaluated by Western blotting. *Fabp7* KO and WT astrocyte were lysed and 10

micrograms of cell lysates were resolved by 15% SDS-PAGE and probed by specific antibodies. Density of bands was analyzed using Multi Gauge software, and β-actin was used as loading control to normalize the loading level of proteins. (**A**) PEA-15 and vimentin expression level were significantly downregulated in *Fabp7* KO astrocytes in comparison with their WT counterparts. No significant change was observed in the expression of GFAP between *Fabp7* KO and WT astrocytes. (**B**) Bar graphs Represent analyses of the relative expression of PEA-15, vimentin, and GFAP in *Fabp7* KO and WT astrocytes analyzed by Mann-Whitney U test. Data are presented as mean ± SEM from two independent Western blotting experiments with at least three biological replicates per genotype; $*P < 0.05$.

4. DISCUSSION

In the present study, I showed for the first time that the dendritic formation of cortical pyramidal neurons, including the complexity of dendritic branching, area covered by the dendritic arbor, and density and maturation of dendritic spines, was reduced in the mPFC of *Fabp7* KO mice. The number of excitatory synapses and their basal activity were also decreased in *Fabp7* KO mice. By using primary neuronal culture systems, I determined that astrocytes expressing FABP7 were critical for these phenotypes. Pyramidal neurons cultured in the ACM derived from *Fabp7* KO astrocytes developed less complex dendritic arbors than those cultured in WT-derived ACM, suggesting that humoral factors secreted from astrocytes were likely involved in the control of this process. Furthermore, rescue of FABP7 expression in the mPFC of *Fabp7* KO mice by transplantation of WT astrocytes partially ameliorated the hyperactive phenotype of *Fabp7* KO mice. Moreover, I presented proteomic differential display analysis of *Fabp7* KO astrocytes compared with WT astrocytes. My findings provide a proof of the principle that FABP7 deficiency can alter the astrocyte proteome. These results strongly suggest that FABP7-mediated astrocytic lipid homeostasis may affect cortical neuronal development; and as the first report of proteomic screening on isolated cells from *Fabp*7 KO mice, suggests the application of such strategies for clarifying the regulatory roles of FABP7 in the brain development and various brain diseases.

Neuronal dendritic and spine development is complex and highly coordinated process (70). In the current study, the formation of neuronal dendrites and their spines was altered in cortical pyramidal neurons of *Fabp7* KO mice. Dendritic spines are the major postsynaptic compartments of excitatory glutamatergic synapses (69), and alteration in spine shape potentially

influences neurotransmission and synaptic plasticity (71). Mature spines (mushroom- and stubby-shaped) are more stable, contain more alpha-amino-3-hydroxy-5-methyl-4-isoxazolepropionic acid (AMPA) glutamate receptors and contribute to the stronger synaptic connections, while immature spines (thin- and filopodium-shaped) are contribute to weak or silent synaptic connections (72). Consistent with reduced number and maturity of dendritic spines, I found the number of excitatory synapses was decreased in the mPFC of *Fabp7* KO mice and in the cortical neurons co-cultured with FABP7-deficient astrocytes. Furthermore, electrophysiological recordings in the cortical pyramidal neurons showed the significant impairment of mEPSCs in *Fabp7* KO mice. Therefore, it is highly possible that functional alterations in astrocytes due to the FABP7 deficiency further disrupted their ability to fully support spinogenesis and synaptogenesis on their neighboring neurons, which leads to the impaired excitatory synaptic activation.

In the current study, I showed that astrocytic FABP7 likely regulates neuronal dendritic and/or spine formation by controlling the production or secretion of humoral factors. It has been shown that the formation of the neuronal dendritic arbor is regulated by intrinsic ability, external signals, or both, and astrocytes provide a number of external cues engaged in the formation and maturation of the dendritic arbor (47). Moreover, astrocytes are able to regulate the number, stability and maturation of dendritic spines (73, 74). Astrocytes secrete several growth factor proteins, such as brain-derived neurotrophic factor, nerve growth factor, neurotrophin-3 (11), ciliary neurotrophic factor and fibroblast growth factor (FGF) (75), which can regulate neuronal growth, differentiation, and maturation (76). Notably, the transfection of *Fabp7* into U87 glioma cells resulted in augmented expression of a number of growth factors, including FGF2 (77), and astrocyte-released FGF2 was shown to promote neurite extension and branching in cerebral

cortical neurons (78). Interestingly, supplementation of culture medium of hippocampal neurons with exogenous FGF2 was shown to increase the number of structurally mature and functionally active excitatory synapses (79). In addition to growth factors, which are proteins, the possible involvement of lipid mediators should be taken into consideration. It is known that lipids including PUFAs promote synaptic plasticity by modulation of synaptic protein expression, and stimulates the dendritic arborization and spines formation (80-83). Neurons are mainly dependent on the lipid molecules that are synthesized and released by glial cells (84). Astrocytes may provide several lipid molecules, although their possible roles in the regulation of neuronal characteristics have received little attention (47). For instance, oleic acid released by astrocytes promoted neurite outgrowth of cortical neurons (85). Considering that FABP7 is a preferential cellular chaperone for n-3 PUFAs (35, 42), impaired uptake, synthesis, and release of n-3 PUFAs would be expected in FABP7-deficient astrocytes. Indeed, we recently reported that uptake of α-linolenic acid, the precursor of DHA, was significantly impaired in *Fabp7* KO astrocytes (34). Therefore, the abnormal neuronal morphology caused by a FABP7 deficiency may also be attributed to the impaired production and release of lipid molecules by astrocytes. Further studies are ongoing to identify the astrocyte-secreted protein and lipid mediators affecting the neuronal plasticity regulated by FABP7.

The mPFC contains profound reciprocal projections to the hippocampus and amygdala (86) and has been associated with a wide scope of behaviors. Miscommunications between these neurons due to impairments in their synaptic inputs can be a major determinant of several cognitive and neurological disorders, including schizophrenia (87), mental retardation (45), autism (88), and Alzheimer's disease (89). Reduced complexity of dendritic branches along with reduced spine density of pyramidal neurons has been reported in the mPFC of patients with

schizophrenia (52, 53). We recently reported that *Fabp7* KO mice show impaired prepulse inhibition (41, 42), a useful endophenotype of schizophrenia (90), and that *FABP7* expression is altered in the mPFC of postmortem schizophrenic brains (41). Notably, we also demonstrated that the frameshift mutant *FABP7* N89fs found in schizophrenia forms cellular aggregates, and the point mutants including *FABP7* S86G and *FABP7* V126L lose their preference for DHA to linoleic acid (42). Although the significance of such mutations in schizophrenia pathology remains unknown, further studies are warranted focusing on the neuronal connections between mPFC and other brain regions in *Fabp7* KO mice and on the relationship between astrocyte lipid metabolism and its involvement in the control of neuronal plasticity.

Previous studies suggested a substantial association of tonic activation in the mPFC with hyperactive behaviors (91). In the present study in accordance with our recent report (42), *Fabp7* KO mice exhibited a hyperactive phenotype, which might mimic some of the positive symptoms of schizophrenia as well as psychomotor agitation (92). I also showed that the transplantation of FABP7-expressing (WT) astrocytes into the mPFC of *Fabp7* KO mice partially rescued the hyperactive phenotype observed in FABP7-deficient mice. Astrocytes have been shown to survive and migrate after grafting and produce trophic factors to enhance neuronal survival, neurite extension, and neuronal function (93). However, little is known about the potential utility of astrocytes for promoting functional recovery. Transplantation of astrocytes was capable of facilitating behavioral recovery in an animal model of Parkinson's disease (94). It was also shown that transplantation of WT or neurotrophin-3 shRNA infected *Fmr1* KO astrocytes into the anterior cingulate cortex of *Fmr1* KO mice (a model of fragile X syndrome) significantly rescued defects in fear memory (95). Moreover, the intra-hippocampal transplantation of astrocyte-restricted neural precursor cells derived from WT mice improved the impairment in

memory performance and long-term potentiation exhibited by IL-1r KO mice (a model of impaired learning, memory and long-term potentiation) (96). Although further study is required to unveil the mechanism, it is likely that the transplanted WT astrocytes affected local neural networks in the mPFC of *Fabp7* KO mice through graft host communication, thereby restoring their behavioral phenotypes.

Here, I showed the decreased expression of PEA-15 in FABP7-deficient astrocytes. PEA-15 is a ubiquitously expressed protein with high levels of expression in astrocytes (97). This protein of low molecular weight (15 kDa) is considered a multi-protein binding molecule serving as an endogenous substrate and molecular adaptor which interacts with various key cellular effectors including protein kinase C (PKC), calcium/calmodulin-dependent protein kinase II (CAM kinase II), Akt, and ERK and thereby modulates major cell functions such as proliferation, apoptosis, and glucose metabolism (97). PEA-15 is involved in epithelial-mesenchymal transition (EMT) (98) and high levels of PEA-15 expression is linked with development of malignancy (97). PEA 15 is reported to be overexpressed in gliomas and mammary carcinomas and may regulate chemoresistance (97). Interestingly, FABP7 is also upregulated in a variety of malignancies, including malignant glioma and mammary carcinoma (99, 100). Furthermore, increased expression of PEA-15 has been reported in reactive astrocytes in postmortem human Alzheimer's disease brain, as well as in the brains of a mouse model of Alzheimer's disease (101) and of amyotrophic lateral sclerosis (102). Consistently, FABP7 is upregulated in reactive astrocytes (34) and is increased in neurodegenerative disorders such as Alzheimer's disease (103, 104). Although the mechanism how FABP7 regulates PEA-15 expression remains to be further studied, it is of note that transcriptional regulation of PEA-15 by peroxisome proliferator-activated receptor gamma (PPARγ), a transcription factor activated by FA-FABP complex, has

been reported (23, 105). Together with the known evidence from the literature, my finding suggests that the known associations of FABP7 with glioma, reactive astrogliosis and neurodegenerative disorders might be partly due to FABP7-mediated regulation of PEA-15 in astrocytes. Further studies on the FABP7-mediated regulation of PEA-15, may highlight the diagnostic or therapeutic potentials of FABP7 in malignancies and other CNS pathologies.

I also showed the decreased expression of vimentin in FABP7-deficient astrocytes. Vimentin is an intermediate filament abundantly expressed in radial glia and immature astrocytes during early development, and it is downregulated towards maturation (106, 107) and is upregualted in reactive astrocytes (108) and glioma (109). This expression pattern highly mimics that of FABP7, suggesting involvement of both molecules in common regulatory networks and supports the FABP7-mediated regulation of vimentin expression. Vimentin is known as a marker for EMT. Overexpression of vimentin is linked with poor prognosis, invasion and tumor growth (110). Known association of vimentin in tumorigenesis in several malignancies including CNS cancers has turned vimentin to an attractive diagnostic and therapeutic target in cancer (110). Thus, FABP7-mediated regulation of vimentin can highlight the diagnostic and therapeutic potentials of FABP7 in malignancies such as glioblastoma. In contrast to vimentin, expression of GFAP did not markedly change in *Fabp7* KO astrocytes as confirmed by Western blotting. Regarding this issue, it has been shown that elevated expression of GFAP and decreased vimentin expression represents astrocytes differentiation (111); vimentin-deficient cells exhibited a slower rate of cell proliferation and DNA synthesis compared with WT cells (112); vimentin-deficient astrocytes were predominantly found to be in G0/G1 stage of cell cycle (113). These data indicate that vimentin downregulation in *Fabp7* KO astrocytes is partly associated with their lower proliferation capacity, and it is interesting to note that *Fabp7* KO astrocytes show the

decreased proliferation compared with WT astrocytes in our previous study (34). Therefore, it is likely that FABP7 is involved in the control of differentiation status of astrocytes possibly through regulation of vimentin expression.

In conclusion, the present study was the first to suggest that FABP7, as an intracellular lipid chaperon expressed by astrocytes, is crucial for the normal development of dendritic arbors and formation/transmission of excitatory synapses in cortical neurons; and as the first proteomic screening on isolated cell cultures from *Fabp7* KO mice, suggests the regulatory roles of FABP7 on the astrocytic expression of PEA-15 and vimentin. Unfortunately, I could not detect any protein candidate known to be involved in the control of neuronal morphological and synaptic plasticity, but these data suggest the regulatory role of FABP7 on astrocyte proteome which should be further evaluated by more accurate quantitative proteomic methods. My findings provide new insights and hypotheses regarding to the association of FABP7 with CNS diseases and may lead to novel therapeutic interventions for such diseases.

REFERENCES

1. Allen NJ & Barres BA (2005) Signaling between glia and neurons: focus on synaptic plasticity. *Current opinion in neurobiology* 15(5):542-548.

2. Seifert G, Schilling K, & Steinhauser C (2006) Astrocyte dysfunction in neurological disorders: a molecular perspective. *Nature reviews. Neuroscience* 7(3):194-206.

3. Taber KH & Hurley RA (2008) Astroglia: not just glue. *The Journal of neuropsychiatry and clinical neurosciences* 20(2):iv-129.

4. Halassa MM & Haydon PG (2010) Integrated brain circuits: astrocytic networks modulate neuronal activity and behavior. *Annual review of physiology* 72:335-355.

5. Powell EM & Geller HM (1999) Dissection of astrocyte-mediated cues in neuronal guidance and process extension. *Glia* 26(1):73-83.

6. Turrigiano GG (2006) More than a sidekick: glia and homeostatic synaptic plasticity. *Trends in molecular medicine* 12(10):458-460.

7. Kettenmann H & Ransom BR (2005) *Neuroglia* (Oxford University Press, New York).

8. Christopherson KS*, et al.* (2005) Thrombospondins are astrocyte-secreted proteins that promote CNS synaptogenesis. *Cell* 120(3):421-433.

9. Mauch DH*, et al.* (2001) CNS synaptogenesis promoted by glia-derived cholesterol. *Science* 294(5545):1354-1357.

10. Nishida H & Okabe S (2007) Direct astrocytic contacts regulate local maturation of dendritic spines. *The Journal of neuroscience : the official journal of the Society for Neuroscience* 27(2):331-340.

11. Rudge JS*, et al.* (1992) Expression of Ciliary Neurotrophic Factor and the Neurotrophins-Nerve Growth Factor, Brain-Derived Neurotrophic Factor and Neurotrophin 3-in Cultured Rat Hippocampal Astrocytes. *The European journal of neuroscience* 4(6):459-471.

12. Ballas N, Lioy DT, Grunseich C, & Mandel G (2009) Non-cell autonomous influence of MeCP2-deficient glia on neuronal dendritic morphology. *Nature neuroscience* 12(3):311-317.

13. Hashimoto K, Shimizu E, & Iyo M (2005) Dysfunction of Glia-Neuron Communication in Pathophysiology of Schizophrenia. *Curr Psychiatry Rev* 1(2):151-163.

14. Jacobs S & Doering LC (2010) Astrocytes prevent abnormal neuronal development in the fragile x mouse. *The Journal of neuroscience : the official journal of the Society for Neuroscience* 30(12):4508-4514.

15. Maragakis NJ & Rothstein JD (2006) Mechanisms of Disease: astrocytes in neurodegenerative disease. *Nature clinical practice. Neurology* 2(12):679-689.

16. Molofsky AV*, et al.* (2012) Astrocytes and disease: a neurodevelopmental perspective. *Genes & development* 26(9):891-907.

17. Moraga-Amaro R, Jerez-Baraona JM, Simon F, & Stehberg J (2014) Role of astrocytes in memory and psychiatric disorders. *Journal of physiology, Paris*.

18. Smathers RL & Petersen DR (2011) The human fatty acid-binding protein family: evolutionary divergences and functions. *Human genomics* 5(3):170-191.

19. Owada Y, Yoshimoto T, & Kondo H (1996) Spatio-temporally differential expression of genes for three members of fatty acid binding proteins in developing and mature rat brains. *J Chem Neuroanat* 12(2):113-122.

20. Owada Y (2008) Fatty acid binding protein: localization and functional significance in the brain. *The Tohoku journal of experimental medicine* 214(3):213-220.

21. Coe NR & Bernlohr DA (1998) Physiological properties and functions of intracellular fatty acid-binding proteins. *Biochimica et biophysica acta* 1391(3):287-306.

22. Storch J & Corsico B (2008) The emerging functions and mechanisms of mammalian fatty acid-binding proteins. *Annual review of nutrition* 28:73-95.

23. Schroeder F*, et al.* (2008) Role of fatty acid binding proteins and long chain fatty acids in modulating nuclear receptors and gene transcription. *Lipids* 43(1):1-17.

24. Kitajka K*, et al.* (2004) Effects of dietary omega-3 polyunsaturated fatty acids on brain gene expression. *Proceedings of the National Academy of Sciences of the United States of America* 101(30):10931-10936.

25. Tan NS*, et al.* (2002) Selective cooperation between fatty acid binding proteins and peroxisome proliferator-activated receptors in regulating transcription. *Molecular and cellular biology* 22(14):5114-5127.

26. Wolfrum C, Borrmann CM, Borchers T, & Spener F (2001) Fatty acids and hypolipidemic drugs regulate peroxisome proliferator-activated receptors alpha - and gamma-mediated gene expression via liver fatty acid binding protein: a signaling path to the nucleus. *Proceedings of the National Academy of Sciences of the United States of America* 98(5):2323-2328.

27. Veerkamp JH & Zimmerman AW (2001) Fatty acid-binding proteins of nervous tissue. *Journal of molecular neuroscience : MN* 16(2-3):133-142; discussion 151-137.

28. Owada Y & Kondo H (2003) Fatty acid binding proteins of the brain. *Cellular Proteins and Their Fatty Acids in Health and Diseases.* , eds Duttaroy A & Spener F (Wiley-VCH,, Weinhem), pp 253-265.

29. Liu RZ, Mita R, Beaulieu M, Gao Z, & Godbout R (2010) Fatty acid binding proteins in brain development and disease. *Int J Dev Biol* 54(8-9):1229-1239.

30. Kurtz A*, et al.* (1994) The expression pattern of a novel gene encoding brain-fatty acid binding protein correlates with neuronal and glial cell development. *Development* 120(9):2637-2649.

31. Owada Y*, et al.* (2006) Altered emotional behavioral responses in mice lacking brain-type fatty acid-binding protein gene. *Eur J Neurosci* 24(1):175-187.

32. Shioda N*, et al.* (2010) Heart-type fatty acid binding protein regulates dopamine D2 receptor function in mouse brain. *The Journal of neuroscience : the official journal of the Society for Neuroscience* 30(8):3146-3155.

33. Sharifi K*, et al.* (2013) Differential expression and regulatory roles of FABP5 and FABP7 in oligodendrocyte lineage cells. *Cell Tissue Res* 354(3):683-695.

34. Sharifi K*, et al.* (2011) FABP7 expression in normal and stab-injured brain cortex and its role in astrocyte proliferation. *Histochem Cell Biol* 136(5):501-513.

35. Balendiran GK*, et al.* (2000) Crystal structure and thermodynamic analysis of human brain fatty acid-binding protein. *The Journal of biological chemistry* 275(35):27045-27054.

36. Matsumata M*, et al.* (2012) The effects of Fabp7 and Fabp5 on postnatal hippocampal neurogenesis in the mouse. *Stem Cells* 30(7):1532-1543.

37. Anthony TE, Mason HA, Gridley T, Fishell G, & Heintz N (2005) Brain lipid-binding protein is a direct target of Notch signaling in radial glial cells. *Genes & development* 19(9):1028-1033.

38. Arai Y*, et al.* (2005) Role of Fabp7, a downstream gene of Pax6, in the maintenance of neuroepithelial cells during early embryonic development of the rat cortex. *J Neurosci* 25(42):9752-9761.

39. Gerstner JR*, et al.* (2008) Brain fatty acid binding protein (Fabp7) is diurnally regulated in astrocytes and hippocampal granule cell precursors in adult rodent brain. *PloS one* 3(2):e1631.

40. Gerstner JR*, et al.* (2012) Time of day regulates subcellular trafficking, tripartite synaptic localization, and polyadenylation of the astrocytic Fabp7 mRNA. *The Journal of neuroscience : the official journal of the Society for Neuroscience* 32(4):1383-1394.

41. Watanabe A*, et al.* (2007) Fabp7 maps to a quantitative trait locus for a schizophrenia endophenotype. *PLoS Biol* 5(11):e297.

42. Shimamoto C*, et al.* (2014) Functional characterization of FABP3, 5 and 7 gene variants identified in schizophrenia and autism spectrum disorder and mouse behavioral studies. *Human molecular genetics*.

43. Urbanska M, Blazejczyk M, & Jaworski J (2008) Molecular basis of dendritic arborization. *Acta neurobiologiae experimentalis* 68(2):264-288.

44. Anderton BH*, et al.* (1998) Dendritic changes in Alzheimer's disease and factors that may underlie these changes. *Progress in neurobiology* 55(6):595-609.

45. Kaufmann WE & Moser HW (2000) Dendritic anomalies in disorders associated with mental retardation. *Cerebral cortex* 10(10):981-991.

46. Harrison PJ (1999) The neuropathology of schizophrenia. A critical review of the data and their interpretation. *Brain : a journal of neurology* 122 (Pt 4):593-624.

47. Barres BA (2008) The mystery and magic of glia: a perspective on their roles in health and disease. *Neuron* 60(3):430-440.

48. Jan YN & Jan LY (2001) Dendrites. *Genes & development* 15(20):2627-2641.

49. Pierce JP, Mayer T, & McCarthy JB (2001) Evidence for a satellite secretory pathway in neuronal dendritic spines. *Current biology : CB* 11(5):351-355.

50. Calabrese B, Wilson MS, & Halpain S (2006) Development and regulation of dendritic spine synapses. *Physiology* 21:38-47.

51. Metz AE, Yau HJ, Centeno MV, Apkarian AV, & Martina M (2009) Morphological and functional reorganization of rat medial prefrontal cortex in neuropathic pain. *Proceedings of the National Academy of Sciences of the United States of America* 106(7):2423-2428.

52. Glantz LA & Lewis DA (2000) Decreased dendritic spine density on prefrontal cortical pyramidal neurons in schizophrenia. *Archives of general psychiatry* 57(1):65-73.

53. Rajkowska G, Selemon LD, & Goldman-Rakic PS (1998) Neuronal and glial somal size in the prefrontal cortex: a postmortem morphometric study of schizophrenia and Huntington disease. *Archives of general psychiatry* 55(3):215-224.

54. Okabe M, Ikawa M, Kominami K, Nakanishi T, & Nishimune Y (1997) 'Green mice' as a source of ubiquitous green cells. *FEBS letters* 407(3):313-319.

55. Numakawa T*, et al.* (2002) Basic fibroblast growth factor evokes a rapid glutamate release through activation of the MAPK pathway in cultured cortical neurons. *The Journal of biological chemistry* 277(32):28861-28869.

56. Xie C, Markesbery WR, & Lovell MA (2000) Survival of hippocampal and cortical neurons in a mixture of MEM+ and B27-supplemented neurobasal medium. *Free radical biology & medicine* 28(5):665-672.

57. Jacobs S & Doering LC (2009) Primary dissociated astrocyte neuron co-culture. *Protocols for neural cell culture*, ed Doering LC (Humana Press, New York), 4th Ed, pp 269–284.

58. Vilalta A & Brown GC (2014) Deoxyglucose prevents neurodegeneration in culture by eliminating microglia. *Journal of neuroinflammation* 11:58.

59. Franklin KBJ & Paxinos G (2008) *The Mouse Brain in Stereotaxic Coordinates* (Academic Press) 3rd Ed.

60. Harris KM (1999) Structure, development, and plasticity of dendritic spines. *Current opinion in neurobiology* 9(3):343-348.

61. Narro ML*, et al.* (2007) NeuronMetrics: software for semi-automated processing of cultured neuron images. *Brain research* 1138:57-75.

62. Ippolito DM & Eroglu C (2010) Quantifying synapses: an immunocytochemistry-based assay to quantify synapse number. *Journal of visualized experiments : JoVE* (45).

63. Kucukdereli H*, et al.* (2011) Control of excitatory CNS synaptogenesis by astrocyte-secreted proteins Hevin and SPARC. *Proceedings of the National Academy of Sciences of the United States of America* 108(32):E440-449.

64. Mitsushima D, Sano A, & Takahashi T (2013) A cholinergic trigger drives learning-induced plasticity at hippocampal synapses. *Nature communications* 4:2760.

65. Tanaka T*, et al.* (2008) Downregulation of two isoforms of ubiquitin carboxyl-terminal hydrolase isozyme L1 correlates with high metastatic potentials of human SN12C renal cell carcinoma cell clones. *Electrophoresis* 29(12):2651-2659.

66. Kuramitsu Y*, et al.* (2009) Proteomic differential display analysis identified upregulated astrocytic phosphoprotein PEA-15 in human malignant pleural mesothelioma cell lines. *Proteomics* 9(22):5078-5089.

67. Wang Y*, et al.* (2014) Proteomic analysis indicates that overexpression and nuclear translocation of lactoylglutathione lyase (GLO1) is associated with tumor progression in murine fibrosarcoma. *Electrophoresis* 35(15):2195-2202.

68. Craig AM & Banker G (1994) Neuronal polarity. *Annual review of neuroscience* 17:267-310.

69. Nimchinsky EA, Sabatini BL, & Svoboda K (2002) Structure and function of dendritic spines. *Annual review of physiology* 64:313-353.

70. Cline HT (2001) Dendritic arbor development and synaptogenesis. *Current opinion in neurobiology* 11(1):118-126.

71. Volfovsky N, Parnas H, Segal M, & Korkotian E (1999) Geometry of dendritic spines affects calcium dynamics in hippocampal neurons: theory and experiments. *Journal of neurophysiology* 82(1):450-462.

72. Matsuzaki M*, et al.* (2001) Dendritic spine geometry is critical for AMPA receptor expression in hippocampal CA1 pyramidal neurons. *Nature neuroscience* 4(11):1086-1092.

73. Garcia O, Torres M, Helguera P, Coskun P, & Busciglio J (2010) A role for thrombospondin-1 deficits in astrocyte-mediated spine and synaptic pathology in Down's syndrome. *PloS one* 5(12):e14200.

74. Haber M, Zhou L, & Murai KK (2006) Cooperative astrocyte and dendritic spine dynamics at hippocampal excitatory synapses. *The Journal of neuroscience : the official journal of the Society for Neuroscience* 26(35):8881-8891.

75. Vaca K & Wendt E (1992) Divergent effects of astroglial and microglial secretions on neuron growth and survival. *Experimental neurology* 118(1):62-72.

76. Ojeda SR, Ma YJ, Lee BJ, & Prevot V (2000) Glia-to-neuron signaling and the neuroendocrine control of female puberty. *Recent progress in hormone research* 55:197-223; discussion 223-194.

77. Kipp M*, et al.* (2011) BLBP-expression in astrocytes during experimental demyelination and in human multiple sclerosis lesions. *Brain, behavior, and immunity* 25(8):1554-1568.

78. Le R & Esquenazi S (2002) Astrocytes mediate cerebral cortical neuronal axon and dendrite growth, in part, by release of fibroblast growth factor. *Neurological research* 24(1):81-92.

79. Li AJ, Suzuki S, Suzuki M, Mizukoshi E, & Imamura T (2002) Fibroblast growth factor-2 increases functional excitatory synapses on hippocampal neurons. *The European journal of neuroscience* 16(7):1313-1324.

80. Rodriguez-Rodriguez RA, Tabernero A, Velasco A, Lavado EM, & Medina JM (2004) The neurotrophic effect of oleic acid includes dendritic differentiation and the expression of the neuronal basic helix-loop-helix transcription factor NeuroD2. *Journal of neurochemistry* 88(5):1041-1051.

81. Sakamoto T, Cansev M, & Wurtman RJ (2007) Oral supplementation with docosahexaenoic acid and uridine-5'-monophosphate increases dendritic spine density in adult gerbil hippocampus. *Brain research* 1182:50-59.

82. Cao D, Xue R, Xu J, & Liu Z (2005) Effects of docosahexaenoic acid on the survival and neurite outgrowth of rat cortical neurons in primary cultures. *The Journal of nutritional biochemistry* 16(9):538-546.

83. Cao D*, et al.* (2009) Docosahexaenoic acid promotes hippocampal neuronal development and synaptic function. *Journal of neurochemistry* 111(2):510-521.

84. Pfrieger FW & Ungerer N (2011) Cholesterol metabolism in neurons and astrocytes. *Progress in lipid research* 50(4):357-371.

85. Tabernero A, Lavado EM, Granda B, Velasco A, & Medina JM (2001) Neuronal differentiation is triggered by oleic acid synthesized and released by astrocytes. *Journal of neurochemistry* 79(3):606-616.

86. Ishikawa A & Nakamura S (2003) Convergence and interaction of hippocampal and amygdalar projections within the prefrontal cortex in the rat. *The Journal of neuroscience : the official journal of the Society for Neuroscience* 23(31):9987-9995.

87. Stephan KE, Baldeweg T, & Friston KJ (2006) Synaptic plasticity and dysconnection in schizophrenia. *Biological psychiatry* 59(10):929-939.

88. Sudhof TC (2008) Neuroligins and neurexins link synaptic function to cognitive disease. *Nature* 455(7215):903-911.

89. Selkoe DJ & Podlisny MB (2002) Deciphering the genetic basis of Alzheimer's disease. *Annual review of genomics and human genetics* 3:67-99.

90. Turetsky BI*, et al.* (2007) Neurophysiological endophenotypes of schizophrenia: the viability of selected candidate measures. *Schizophrenia bulletin* 33(1):69-94.

91. Jodo E (2013) The role of the hippocampo-prefrontal cortex system in phencyclidine-induced psychosis: a model for schizophrenia. *Journal of physiology, Paris* 107(6):434-440.

92. Jones DNC, Gartlon JE, Minassian A, Perry W, & Geyer MA (2008) Developing newdrugs for schizophrenia: fromanimals to the clinic. *Animal and translational models for*

cns drug discovery: psychiatric disorders., eds McArthur R & Borsini R (Elsevier, New York), pp 199-262.

93. Huang H, Chen L, & Sanberg P (2010) Cell Therapy From Bench to Bedside Translation in CNS Neurorestoratology Era. *Cell medicine* 1(1):15-46.

94. Bradbury EJ, Kershaw TR, Marchbanks RM, & Sinden JD (1995) Astrocyte transplants alleviate lesion induced memory deficits independently of cholinergic recovery. *Neuroscience* 65(4):955-972.

95. Yang Q*, et al.* (2012) Excessive astrocyte-derived neurotrophin-3 contributes to the abnormal neuronal dendritic development in a mouse model of fragile X syndrome. *PLoS genetics* 8(12):e1003172.

96. Ben Menachem-Zidon O*, et al.* (2011) Astrocytes support hippocampal-dependent memory and long-term potentiation via interleukin-1 signaling. *Brain, behavior, and immunity* 25(5):1008-1016.

97. Fiory F, Formisano P, Perruolo G, & Beguinot F (2009) Frontiers: PED/PEA-15, a multifunctional protein controlling cell survival and glucose metabolism. *Am J Physiol Endocrinol Metab* 297(3):E592-601.

98. Lee J*, et al.* (2012) PEA-15 unphosphorylated at both serine 104 and serine 116 inhibits ovarian cancer cell tumorigenicity and progression through blocking beta-catenin. *Oncogenesis* 1:e22.

99. Kaloshi G*, et al.* (2007) FABP7 expression in glioblastomas: relation to prognosis, invasion and EGFR status. *J Neurooncol* 84(3):245-248.

100. Liu RZ*, et al.* (2012) A fatty acid-binding protein 7/RXRbeta pathway enhances survival and proliferation in triple-negative breast cancer. *J Pathol* 228(3):310-321.

101. Thomason LA, Smithson LJ, Hazrati LN, McLaurin J, & Kawaja MD (2013) Reactive astrocytes associated with plaques in TgCRND8 mouse brain and in human Alzheimer brain express phosphoprotein enriched in astrocytes (PEA-15). *FEBS Lett* 587(15):2448-2454.

102. Sharif A*, et al.* (2004) The expression of PEA-15 (phosphoprotein enriched in astrocytes of 15 kDa) defines subpopulations of astrocytes and neurons throughout the adult mouse brain. *Neuroscience* 126(2):263-275.

103. Guttula SV, Allam A, & Gumpeny RS (2012) Analyzing microarray data of Alzheimer's using cluster analysis to identify the biomarker genes. *Int J Alzheimers Dis* 2012:649456.

104. Prinzen C*, et al.* (2009) Differential gene expression in ADAM10 and mutant ADAM10 transgenic mice. *BMC Genomics* 10:66.

105. Ungaro P*, et al.* (2012) Peroxisome proliferator-activated receptor-gamma activation enhances insulin-stimulated glucose disposal by reducing ped/pea-15 gene expression in skeletal muscle cells: evidence for involvement of activator protein-1. *J Biol Chem* 287(51):42951-42961.

106. Gomes FC, Paulin D, & Moura Neto V (1999) Glial fibrillary acidic protein (GFAP): modulation by growth factors and its implication in astrocyte differentiation. *Braz J Med Biol Res* 32(5):619-631.

107. Lepinoux-Chambaud C & Eyer J (2013) Review on intermediate filaments of the nervous system and their pathological alterations. *Histochem Cell Biol* 140(1):13-22.

108. Sofroniew MV (2009) Molecular dissection of reactive astrogliosis and glial scar formation. *Trends Neurosci* 32(12):638-647.

109. Tso CL*, et al.* (2006) Primary glioblastomas express mesenchymal stem-like properties. *Mol Cancer Res* 4(9):607-619.

110. Satelli A & Li S (2011) Vimentin in cancer and its potential as a molecular target for cancer therapy. *Cell Mol Life Sci* 68(18):3033-3046.

111. Svechnikova I, Almqvist PM, & Ekstrom TJ (2008) HDAC inhibitors effectively induce cell type-specific differentiation in human glioblastoma cell lines of different origin. *International journal of oncology* 32(4):821-827.

112. Wang N & Stamenovic D (2000) Contribution of intermediate filaments to cell stiffness, stiffening, and growth. *American journal of physiology. Cell physiology* 279(1):C188-194.

113. Gillard BK*, et al.* (1998) Decreased synthesis of glycosphingolipids in cells lacking vimentin intermediate filaments. *Experimental cell research* 242(2):561-572.